ACCESS
Arctic Climate Change
Economy and Society

Project no. 265863

ACCESS

Arctic Climate Change, Economy and Society

Instrument: Collaborative Project
Thematic Priority: Ocean.2010-1 "Quantification of climate change impacts on economic sectors in the Arctic"

D1.27 – Report on Autonomous Underwater Vehicle Missions (WP3)

Due date of deliverable: **30/04/2014**
Actual submission date: **17/03/2015**

Authors: Peter Wadhams (Department of Applied Mathematics and Theoretical Physics, University of Cambridge), Bo Krogh (Bo Krogh ApS), Richard Yeo (AUV Consultants), Stephen Moelvig (COWI ApS), John Fletcher (University of Cambridge), Robin Clancy (University of Cambridge), Charlie Hogg (University of Cambridge), Till Wagner (University of Cambridge), Hanumant Singh (Woods Hole Oceanographic Institute)

Start date of project: **March 1st, 2011** Duration: **48 months**
Organisation name of lead contractor for this deliverable: **UCAM**

Project co-funded by the European Commission within the Seventh Framework Programme (2007-2013)		
Dissemination Level		
PU	Public	X
PP	Restricted to other programme participants (including the Commission Services)	
RE	Restricted to a group specified by the consortium (including the Commission Services)	
CO	Confidential, only for members of the consortium (including the Commission Services)	

Table of Contents

PART I: MAPPING OF ICE THICKNESS AND PRESSURE RIDGE SHAPES IN THE FRAM STRAIT IN SUMMER 2011 AND 2012

CHAPTER 1: INTRODUCTION 4

CHAPTER 2: SUMMARIES 4

2.1 AS11 4
2.2 AS12 6

CHAPTER 3: MEASUREMENTS/RESULTS 8

3.1 AUV DATA 8
3.2 LIDAR 14
3.3 DRILL LINES 18
3.4 AERIAL IMAGING 20

CHAPTER 4: DISCUSSION 23

4.1 AUV 23
4.2 LIDAR 24
4.3 DRILL DATA 25

PART II: MAPPING OF ICE THICKNESS AND PRESSURE RIDGE SHAPES IN THE BEAUFORT SEA IN SUMMER 2014

CHAPTER 1: INTRODUCTION AND PURPOSE OF WORK 27

CHAPTER 2: FRAMEWORK OF EXPEDITION INVOLVED 27

CHAPTER 3: DESCRIPTION OF EQUIPMENT 28

3.1 THE GAVIA AUV 28
3.2 USBL TRANSPONDER TRACKING SYSTEM 28
3.3 QUADCOPTER 31

CHAPTER 4: MOBILISATION FOR VOYAGE 32

CHAPTER 5: DESCRIPTION OF OPERATIONS 32

5.1 VOYAGE FROM SEWARD TO BEAUFORT SEA 32
5.2 PRELIMINARY TRIALS (AUG 16 AND 17): RESULTS AND PROBLEMS 33
5.3 FIRST EXPERIMENT, AUGUST 18 34
5.4 SECOND AND THIRD EXPERIMENT, AUGUST 19 36
5.5 AUV DRAFT MEASUREMENTS 37
5.3 WAVE BUOY INTERACTIONS AUGUST 20 43

CHAPTER 6: RESULTS OF MAPPING OPERATIONS 44

CHAPTER 7: CONCLUSIONS ON PROPERTIES AND TOPOGRAPHY OF MELTING ICE 44

REFERENCES 46

APPENDIX: AS11 DRILL LINE PROFILES 47

SUMMARY

In part I we report on field experiments and results achieved during experiments in Fram Strait from R.V. "Arctic Sunrise" carried out in the summers of 2011 and 2012. The 2011 experiments involved high-resolution mapping of the upper ice surface using a laser scanning system supplied by Scan Lab Ltd. These experiments were repeated in 2012 but with the addition of an AUV (autonomous underwater vehicle) rented from Woods Hole Oceanographic Institution, and equipped with a Geoswath multibeam sonar to record the three-dimensional structure of the ice underside. The collocation of the high-resolution measurements of the ice upper and lower side in selected pressure ridges permits not only an unprecedented quality of measurement of pressure ridge morphology but also a large number of accurate freeboard-draft correlations which are important for validation of satellite borne ice thickness measuring systems such as the CryoSat-2 radar altimeter. One of the ridges sampled in this way was a type of ridge never before mapped quantitatively, a stamukha, or large, thick (28 m draft) isolated ridge which has spent a number of summers aground on the Siberian shelf before melting enough to drift off the seabed and join the moving pack. It could be identified by its exceptionally low salinity and covering of dirt, from Siberian river overflows.

In part II we report observations of ice thickness and pressure ridge shapes in the Beaufort Sea in summer 2014 from the USCGC Healy. Three successful datasets were acquired with the Gavia AUV. Two of the floes observed (2014A and 2014B) showed ice with few large blocks. One floe (2014D) showed more coherent, linear ridge structures. We found that in the summer melt conditions observed, the ridges were broken up into individual blocks. The remnant ridges retained a significant proportion of the ice volume.

PART I: MAPPING OF ICE THICKNESS AND PRESSURE RIDGE SHAPES IN THE FRAM STRAIT IN SUMMER 2011 AND 2012

Chapter 1: Introduction

New record minima of sea ice are being reported year after year. The data behind these results stems almost exclusively from satellite mounted radars. Modern satellite technology is very accurate in measuring the surface area covered by sea ice, but still struggles to reliably measure the thickness of the highly variable ice cap. Up to now, satellite measurements appear to be biased in that they get more returns from bigger floes. The relation between floe size and thickness in the MIZ is thus of crucial interest, as one example. The data set collected during this project (with its large number of floes) will provide an excellent opportunity to study this relation, amongst others.

As the Arctic ice retreats further, the traditional idea of the Arctic sea ice as being strongly confined by surrounding landmass begins to lose justification. Over the coming years the ice pack will be increasingly subjected to divergent wind and current stresses, which will lead to a thinner and more loosely packed ice regime - resembling the seasonal sea ice cover of the Southern Ocean. In order to get a complete characterization of the ice, comparison of high resolution surface topography data and corresponding underside scans are called for. To achieve this we tested the surface LiDAR scanning equipment during a trial cruise in 2011 and added AUV-mounted multibeam sonar during a follow-up expedition in 2012. This means not only a more complete survey but also a temporal continuity that will help understand the evolution of the ice over time. The BAS ICEBELL cruise (2010) to the Weddell and Bellingshausen Seas collected a similar data set, as well as the SIPEX-II cruise in September- November 2012 to the East Antarctic. Not only being of great scientific value in their own right, comparing these data sets will be a first step in finding out whether the Arctic is approaching the conditions of the Antarctic.

Chapter 2: Summaries

2.1 AS11

In September 2011, the authors led a research expedition (henceforth: AS11) to Fram Strait aboard “Arctic Sunrise” to monitor sea ice conditions. Our purpose was twofold: a) help validate and calibrate satellite measurements in the marginal ice zone (MIZ) and b) gather high resolution data of deformed sea ice that will provide new insights into the physical processes underlying sea ice mechanics and dynamics. This was mainly designed to be a test-run for a more comprehensive cruise (see next section). In order to achieve these goals we performed a variety of observations, including ice core sampling, snow depth measurements, thickness readings, aerial imagery and 3D laser scanning. A total of 17 ice floes were surveyed. The final data set includes 77 panoramic 3D laser scans, over 350 ice thickness measurements and several thousand aerial images.

Three sets of observations were conducted, with 3-10 floes at each site. The first period of observations took place between Sept 4-11 at 80°40’ - 80°50’N/1°15’E-1°25’E. Three floes were measured on this leg of the experiment. Detailed scans, representative drill-lines (10-20 holes) and corresponding snow depths were collected, as well as ice-core samples for floes 1 and 2. After a brief return to Longyearbyen, Svalbard, to exchange personnel, the second leg of the experiment took place from Sept 15-18 around 79°15’-35’N/2°E-3°28’W. On floes 4 and 6 a large number of scans was

performed (12 and 24, respectively), together with extensive drilling lines (41 holes/4 lines, 51 holes/5 lines, respectively) to give detailed topographies of the floes at hand. On Sept 16, a small crew of 3 scientists measured five small floes (5A-E) in the vicinity of the ship to obtain a representative picture of the ice conditions in this region of the marginal ice zone. The scientists were dropped on the (pseudo-)randomly chosen floes by helicopter to collect a single scan and a drill line (5-8 holes) on each floe. On Sept 17, two scientists and one crew member flew north, stopping at intervals of ca. 10 nm, to measure the evolution of ice thickness from the ice edge northwards. Drill lines were obtained on four different floes (7A-D), with approximately 10 holes each, apart from floe 7D, a MY floe, which featured average thicknesses of ~4m, so that after 4 holes the crew returned to the ship due to time constraints. After another stopover in Longyearbyen, the third leg of the cruise took place on Sept 21/22 close to the location of the second (at 79°8'-11'N/0°20'W-4°27'W). Due to foggy conditions with little visibility and repeated sightings of polar bears in the vicinity of the ship, the time spent collecting data was limited on this last leg. However, a total of 103 drill holes (6 lines) and 3 scans could be obtained on floe 9, as well as 3 high resolution scans and a 12-hole drill line on floe 10. In general throughout this cruise, the floes measured were chosen to give a representative picture of the of the local ice conditions - with exception of floes 3 and 6 which were selected for their intricate topographies.

The collected data are presented and discussed in section 3.

Date	Floe	Lat/Lon	Scanner	Drill Data	Imagery	Survey Data	Snow Depths	Cores
03/09	1	80º 42.9' N, 2º 25.5' E	8	23 (ALine)	✓	27 (Random)	30 (ALine)	1
04/09 05/09	2[a]	80 º 43.1' N, 2º17.0' E	11	12 (ALine) 11 (BLine) 12 (Cline)	✓	78(Aline +) 108 (BLine+Peri)	31 (ALine) 61 (‖ ALine) 114 (→ Survey)	2
09/09 – 11/09	3[b]	80º 52.1' N 1º 27.7' E	6	22 (ALine)	-	279(ALine+Peri)[c] 1012 (Grid)	16 (ALine) 14 (Random)	-
15/09	4	79º 38.3' N, 2º 02.6' E	12	11 (ALine) 11 (BLine) 8 (CLine) 11 (DLine)	✓	-	No signif. snow	1
16/09	5A 5B 5C 5D 5E	79º 26.4' N, 2º 31.8' W	2 1 1 1 2	8 (5m int.) 6 (") 6 (") 5 (") 5 (")	✓	-	-	-
17/09 18/09	6	79º 16.5' N, 3º 28.3' W	24	11 (ALine) 22 (BLine) 18 (CLine)	✓	-	No signif. snow	3
17/09	7A[d] 7B 7C 7D	79º 23.9N, 3º 47.3' W 79º 32.5N, 4º 08.0'W 79º 43.4'N, 4º 18.2'W 79º 55.4'N, 4º 17.5'W	-	10 (5m int.) 11 (") 10 (") 4 (")	✓	-	-	-
18/09	8	79º 06.3' N, 3º 42.8' W	3	9 (5m int.)	-	-	No signif. snow	1
21/09	9	79º 8.2'N, 0º, 20.4'W	3	103 (6 Lines)	✓	110 (6 Lines)	110 (6 Lines)	1
22/09	10	79º 11.4'N, 4º 27.4'W	3 (hi-res)	12 (ALine)	-	16 (ALine)	16 (ALine)	-

Table 1: Overview of measurements taken during AS11

a) Floe 2 broke up into 2 pieces halfway through drilling the ALine

b) Floe 3 broke up into 2 pieces after the 9th

c) First set of survey points taken on 09/09, second set taken on 10/09 after breakup

d) Floe 7 was measured every 10 nm going north from the ship (Floe 6)

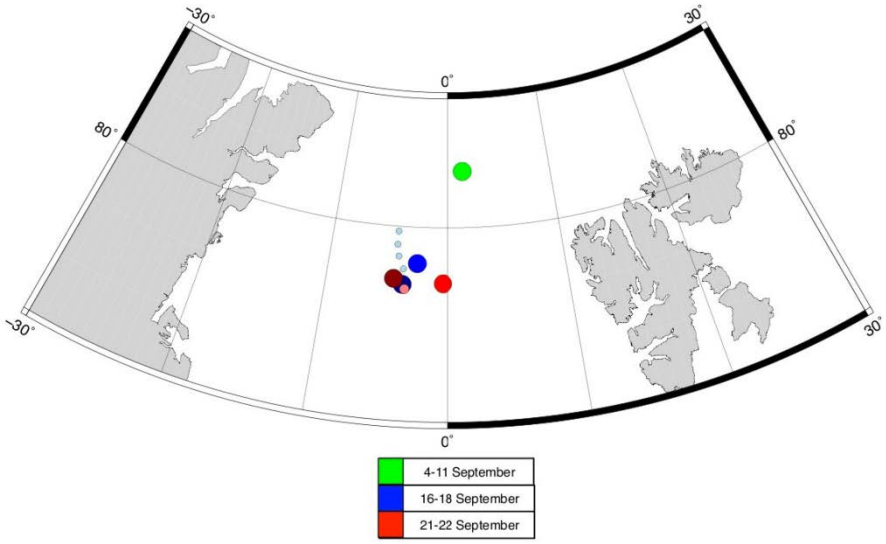

Figure 1: Map of locations visited during field experiment AS11.

2.2 AS12

A second field operation, this time to measure simultaneously the surface and underside topography of pressure ridges, was carried out between July 9 and 21 2012, again using MV "Arctic Sunrise" by courtesy of Greenpeace. DAMTP personnel were Prof Peter Wadhams (chief scientist), postdoc John Fletcher and graduate students Till Wagner and Nick Toberg. The underside was profiled by a Sea Bed AUV of Woods Hole Oceanographic Institution, which was operated by Dr Hanu Singh and two assistants. The surface topography was obtained in high resolution by Laser Scan (William Trussell).

The ship started from Longyearbyen, where the AUV was calibrated and tested, on July 10, and sailed to meet the ice edge in Fram Strait at a location (79° 32'N, 0° 40'E) corresponding to a Radarsat quadpol retrieval expected on July 14 and ordered by the Norwegian Meteorological Institute (Nick Hughes) as part of their participation in Sidarus. The ship was in 50% concentration first-year (FY) and multi-year (MY) floes when it reached this position.

The first floe selected, floe 1, was a large, long MY floe carrying a classic triangular ridge, a low rolling hummock and a lot of rubble. The ship was moored to the floe, the Laser Scan operation carried out as well as several cores drilled, and several lines of thickness holes drilled, in order to obtain optimal co-registration between laser and AUV.

Floe 2, in the same vicinity, was a **stamukha**, a very old isolated pressure ridge, covered in dirt and of considerable draft (28 m), which is a feature of the shelf seas north of Siberia. They are ridges which run aground and remain fast to the seabed through a summer when all the ice around them melts, leaving the stamukha as a grounded isolated island. It may remain for a number of years at a given site (typically a coastal site on the Siberian shelf) before lifting off through melt and joining the Arctic circulation, to emerge through Fram Strait as a real rarity. To our knowledge no stamukha has been studied before in this intense way, and once again we were able to obtain AUV multibeam mosaics of the underside and laser scans of the topside.

Floe 3, on July 16, had a well developed ridge complex on one edge of a very large (2 km) floe. The

first AUV transit was successful, but a second mosaic resulted in the vehicle being carried into the centre of the floe through not having sufficient power to stem a strong relative current moving under the floe. The AUV was lost and could not be recovered despite a day of searching; it was insured by WHOI.

Floe 4 was mapped only on the upper surface by the laser, with drilled and cored holes. It was overflown at low level by the Basler Polar 5 aircraft of Alfred Wegener Institute on July 18, equipped with an EM-31 electromagnetic ice thickness profiling system.

Finally, floe 5 was profiled by laser and found to be a thick FY floe with well-defined linear ridges. This was the floe which was profiled by the AWI aircraft.

All floes had lines of holes drilled across them to provide a tie-in between the surface and bottom topographies recorded by the two types of instrument. Floe locations were chosen so as to be within the range of successive Radarsat quadpol retrievals, to be monitored and analysed by Nick Hughes at Norwegian Meteorological Institute.

Date	Floe	Lat/Lon	AUV	#Scans	#Drill Data	#Snow Data
14/07	2[a]	79º 43.019' N, 0º 26.704' E	Yes	11	-	N/A
15/07	3	79º 48.125'N, 0º 12.442' E	Yes[b]	9	41	41
16/07	4	79º 50.091' N, 0º 29.350' E	Yes[c]	11	12	9
19/07	5	79º 30.016' N, 0º 02.785' W	No	8	13 x 4 (lines)	13 x 4 (lines)

Table 2: Overview of measurements taken during AS12

a) Stamukha – the floe was too thick for manual drilling, no significant snow

b) AUV track deviated from original route due to strong sub-surface currents

c) AUV completed square survey, again slight deviations due to currents

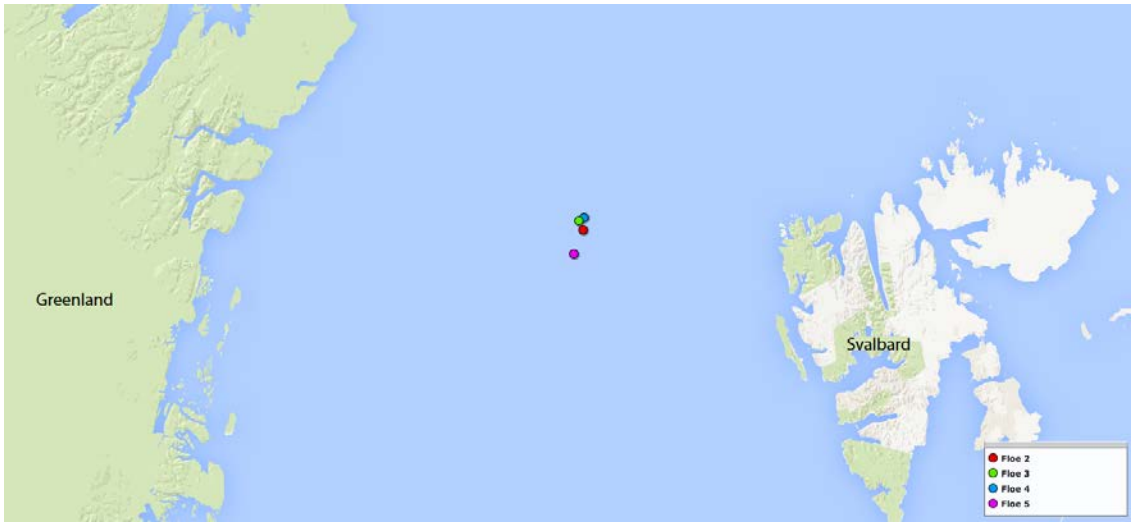

Figure 2: Map of the locations visited during field experiment AS12.

Chapter 3: Measurements/Results

3.1 AUV data

Multibeam sonar data measured by the AUV for floes 1, 2 and 3 of AS12 are presented in figures 3, 4 and 5 respectively. In the case of floe 1 and 3, coverage across the floe is somewhat sporadic, however individual sections have been identified which have reasonable coverage and potentially interesting features.

To remove noise in the data and compensate for its non-uniform spatial distribution, a number of steps were taken to process the data. The data were vertically adjusted a small amount such that a hopefully more accurate sea surface level was represented. Filtering was then performed to remove negative draft values and typically the top 1% of draft values. Finally an interpolation and smoothing process was performed to remove noise, which tended to be in the form of ”streaks” in the data. The processed data are presented in figures 6, 7 and 8.

Floe 1 had generally fairly poor data coverage, however three useable sections were identified (1A, 1B and 1C, shown in figure 3). Figure 6 shows 2D and 3D representations of these sections after processing.

The western side of section 1A contains a block or ridge of dimensions of approximately 15 m by 5 m, with depths exceeding 5 m. There is evidence of further thick ice towards the edge of the data coverage to the west and south-west, where drafts are in excess of 3 m. The east of section 1A appears to be comprised of thinner, undeformed ice, generally around 2 m in depth.

Section 1B contains a large, but relatively shallow ridge with drafts of 2-3 m. There rest of the section appears to be comprised of open water or very thin ice, other than one or two smaller ridges or blocks of ice.

The data in section 1C does not show many clearly defined, linear features, however there does appear to be evidence of some deformation and rubble extending to depths of up to 3 m.

Floe 2 contains the most congruous data of all the floes, with a continuous swathe over a roughly 50 m^2 area. The shape of the underside of the stamukha shown in figure 8 appears to be well defined. The draft reaches a depth around 28 m at its maximum, falling to 14 m in the centre of the section before rising again above 25m to the south of the section.

Similar to floe 1, floe 3 contains a large gap in data coverage in its centre. There are, however, a greater number of usable sections of data with features of interest, identified as 3A, 3Bi, 3Bii, 3C and 3D.

Section 3A appears to contain a distinct ridge, however in the centre of this ridge are patches of anomalously low draft values and missing data, which draws into question the reliability of the data within this section. If accurate, the data suggests that the ridge is fairly large and peaks at a draft of 6 m. The west edge of the section is dominated by thicker, deformed ice, while the ice to the east of the section is much thinner.

Section 3B is comprised of two sections (3Bi and 3Bii). These sections both contain ridges or blocks which might both belong to one continuous, linear feature. The ridge in section 3Bi extends to depths of around 5 m, however it is not perfectly linear and appears to be made of a number of smaller blocks. While the ridge in 3Bii is of a similar depth, it is more clearly linear and symmetrical than the ridge in 3Bi. The sides of the ridge in 3Bii are also steeper, so much so that they may be an artifact of ”streaks” in the unprocessed data, most of which were removed in the smoothing process.

Section 3C appears to contain a number of small blocks, with a maximum depth of around 3 m. Together, these blocks form part of a rubble field. There is some evidence of a linear feature through the centre of this section, including the two largest blocks and a lead to the south of this. If this is the case then the feature has clearly been heavily eroded.

Section 3D still shows some strong signs of the previously mentioned “streaks” in the data, which could not be removed without excessive smoothing. Despite this, it is still possible to make out some features, such as the large mass of ice 3.5 to 4 m thick in the south west of the section and two to three smaller, blocky features in the centre of the section, which have drafts up to 3.5 m.

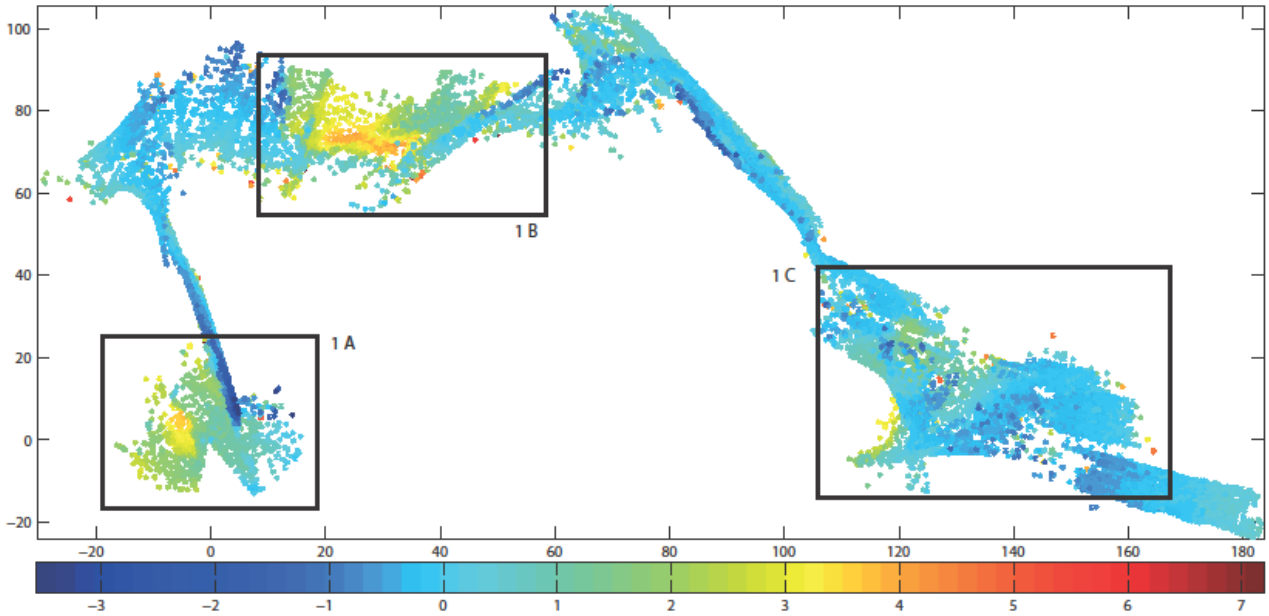

Figure 3: Map showing the unprocessed multibeam AUV data from floe 1 of AS12. The x and y axes are in metres and the colour bar represents draft in metres. The subsections of the floe analysed in greater details are outlined by black boxes.

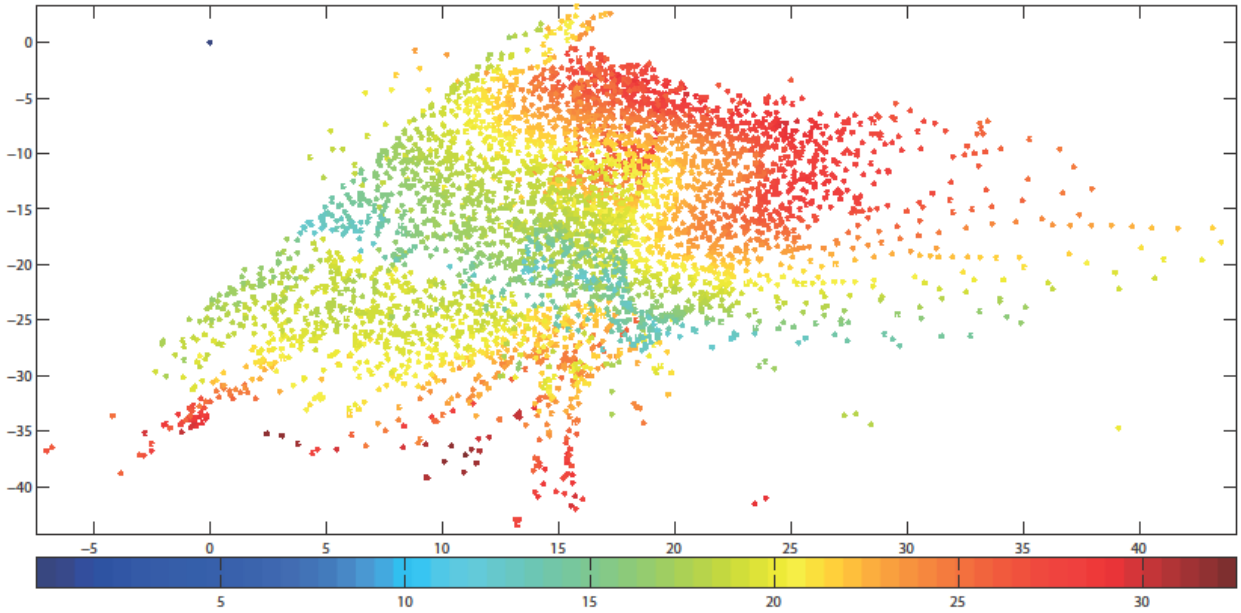

Figure 4: Map showing the unprocessed multibeam AUV data from floe 2 of AS12. The x and y axes are in metres and the colour bar represents draft in metres.

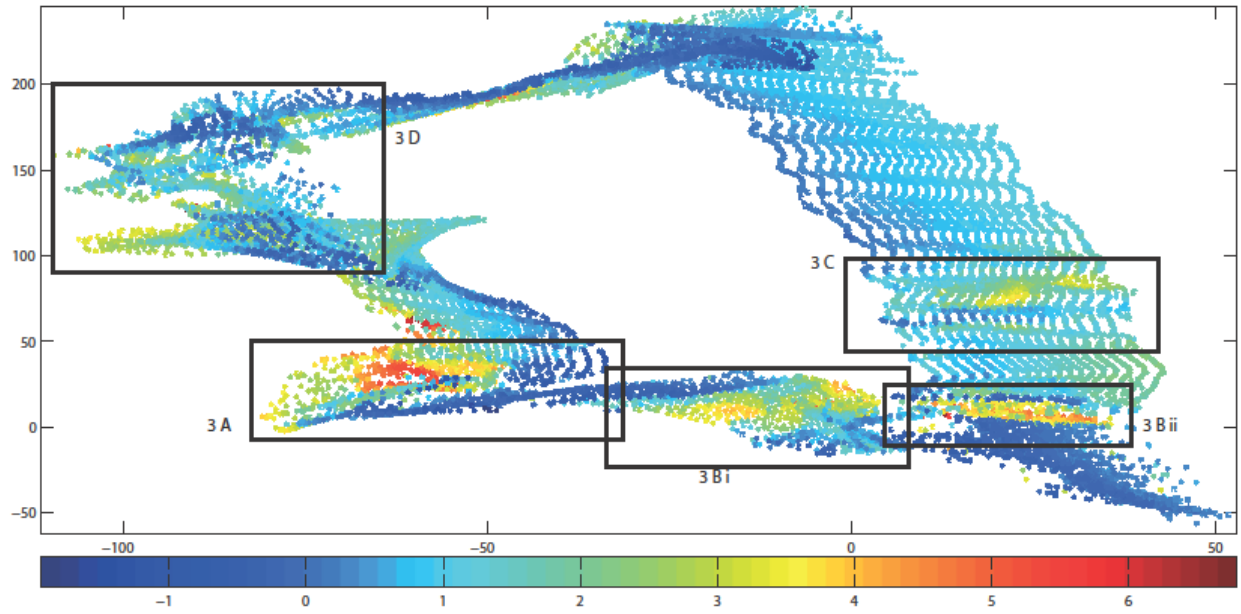

Figure 5: Map showing the unprocessed multibeam AUV data from floe 3 of AS12. The x and y axes are in metres and the colour bar represents draft in metres. The subsections of the floe analysed in greater details are outlined by black boxes.

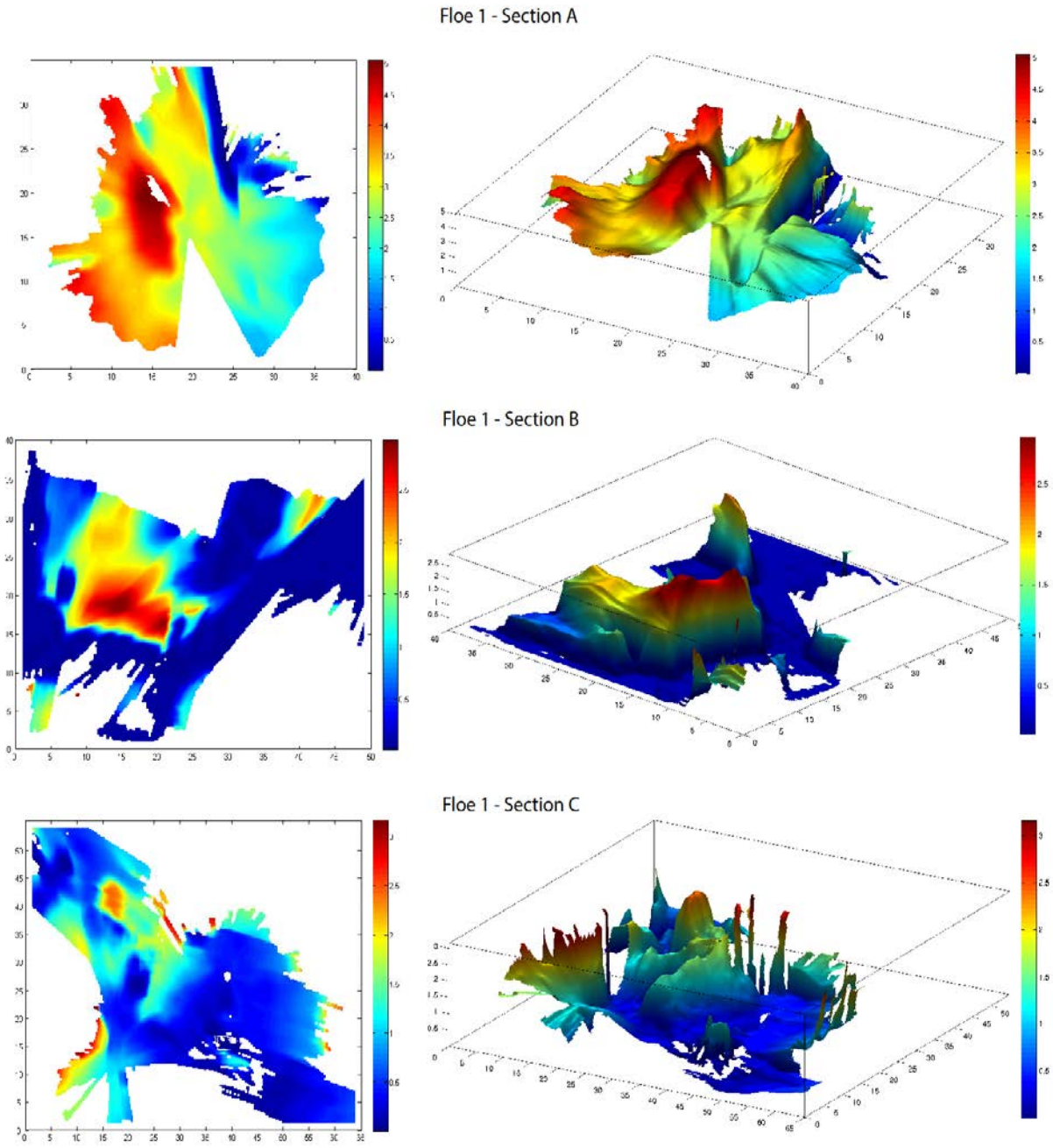

Figure 6: Multibeam AUV data from floe 1 of AS12. 2D and 3D representations are given. The x and y axes are in metres. The z axis and colour bar represent draft (inversted for 3D plots) in metres.

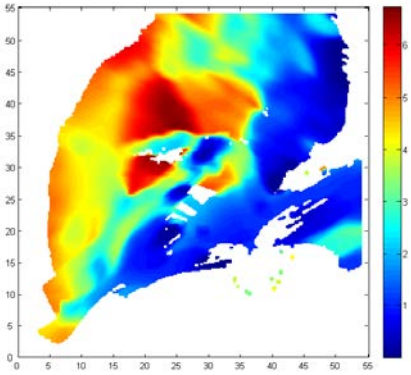

3 A

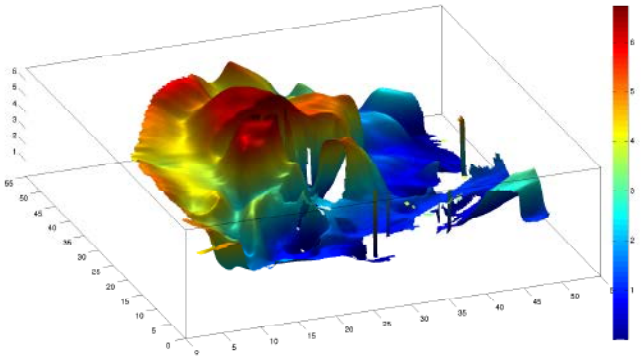

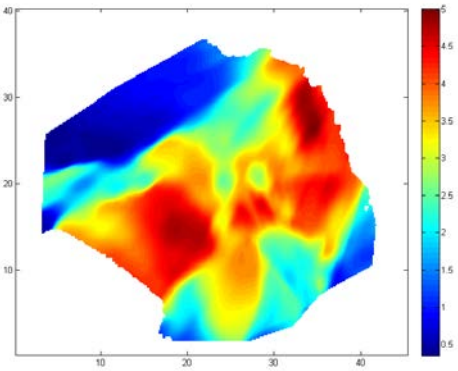

3 B i

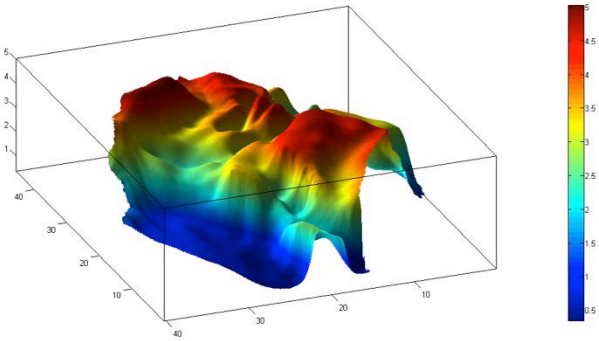

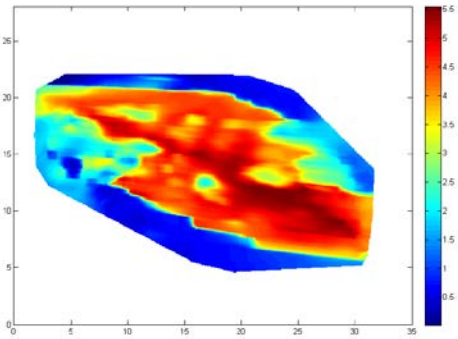

3 B ii

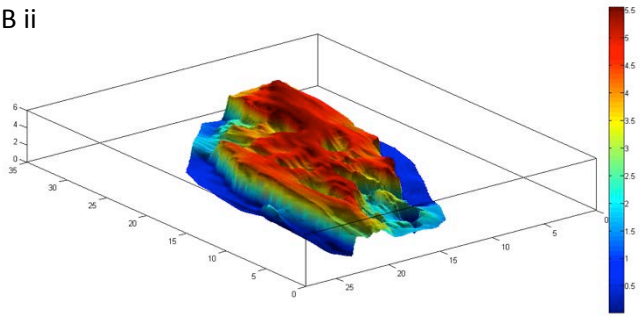

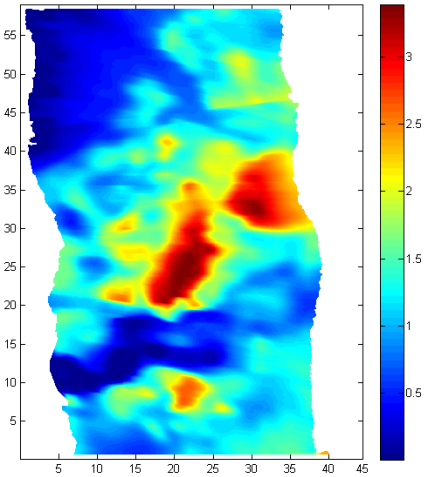

3 C

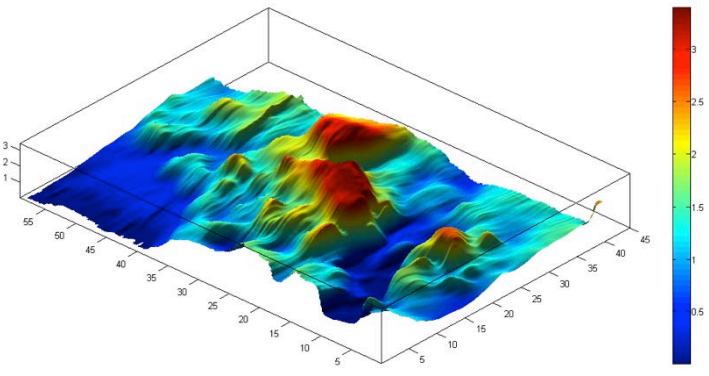

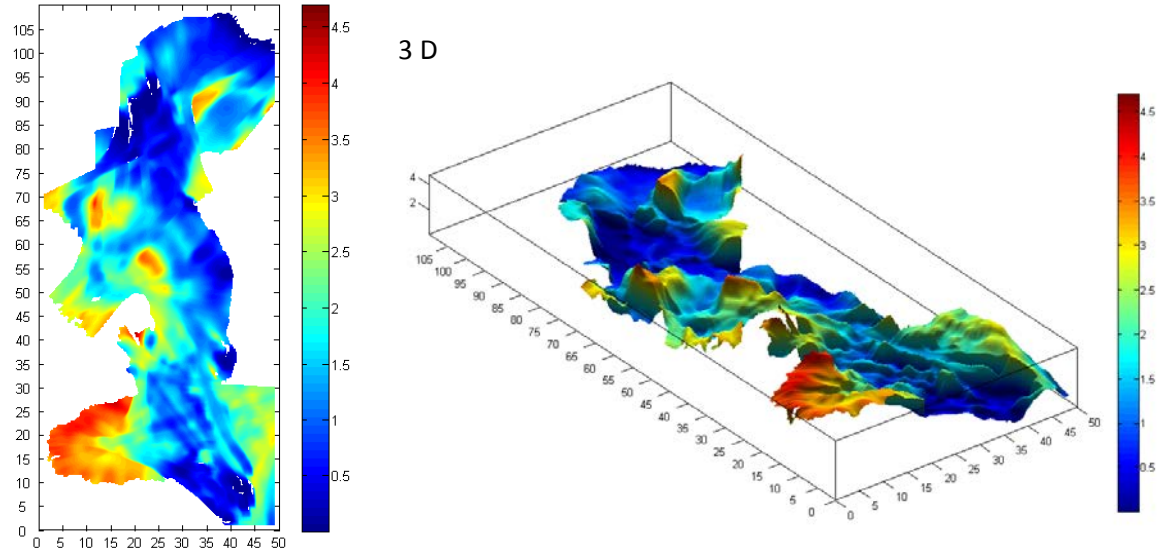

Figure 7: Multibeam AUV data from floe 3 of AS12. 2D and 3D representations are given. The x and y axes are in metres. The z axis and colour bar represent draft (inverted for 3D plots) in metres.

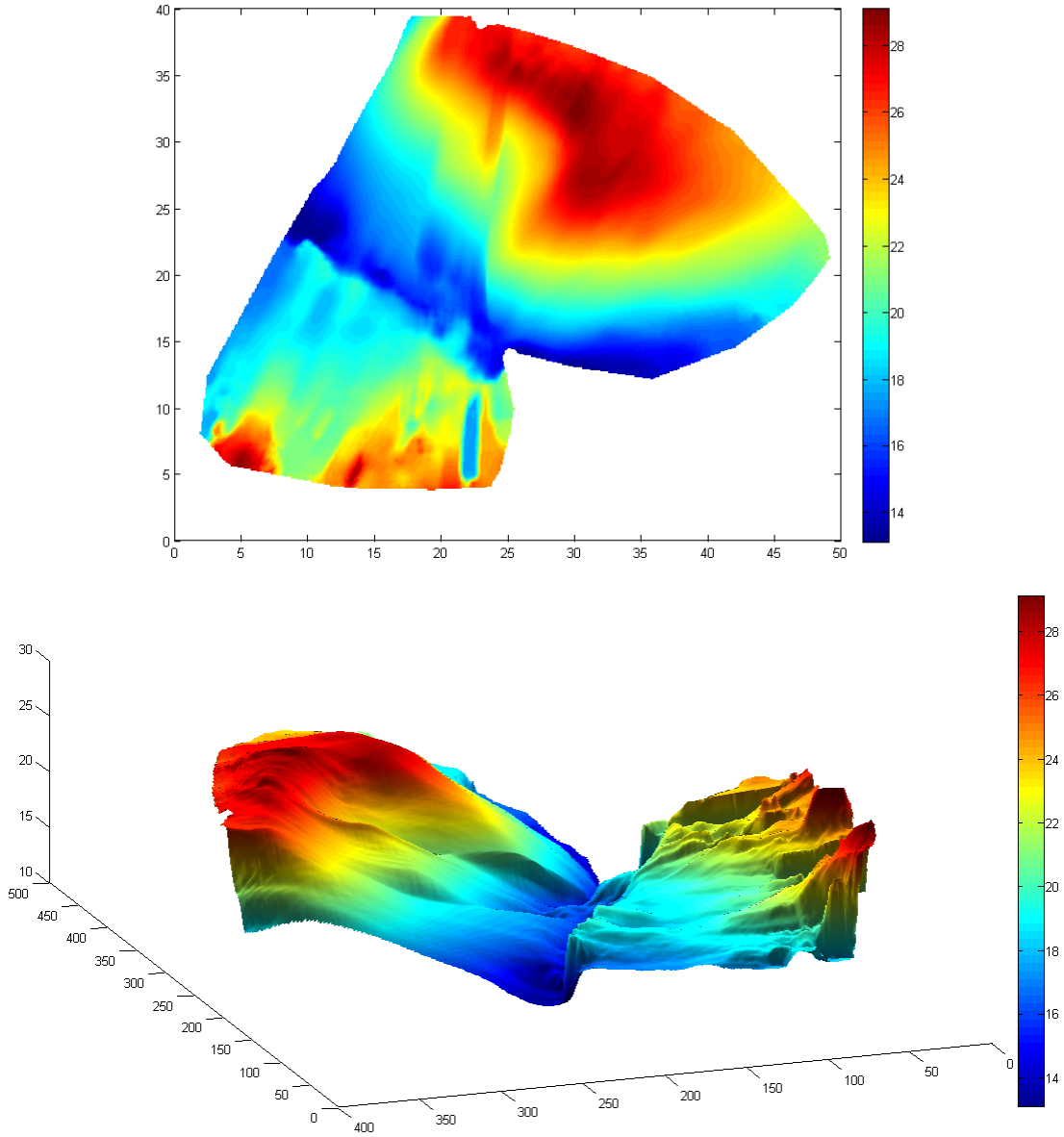

Figure 8: Multibeam AUV data from floe 2 of AS12. 2D and 3D representations are given. The x and y axes are in metres. The z axis and colour bar represent draft (inversted for 3D plots) in metres.

3.2 LiDAR

In an Arctic first, 3D scanning experts worked with sea ice scientists in situ to make the best use of state-of-the-art laser technology. The 3D replica of the ice surface produced provides information on pressure ridge topography and melt pond sizes and shapes as well as snow drift patterns and individual ice block characteristics.

In total, 10 floes were scanned as a part of AS11 and 5 more during AS12. An overview of these scans is presented in figure 9. Data from the scans of the AS12 floes is shown in figures 10 and 11. A number of features are visible in figure 10, including ridges, rubble and leads. The topography of the stamukha is also well captured in figure 11. An example of how different ice morphologies can be differentiated using the LiDAR data is included in figure 12, as are probability density functions of the freeboard for each morphology identified.

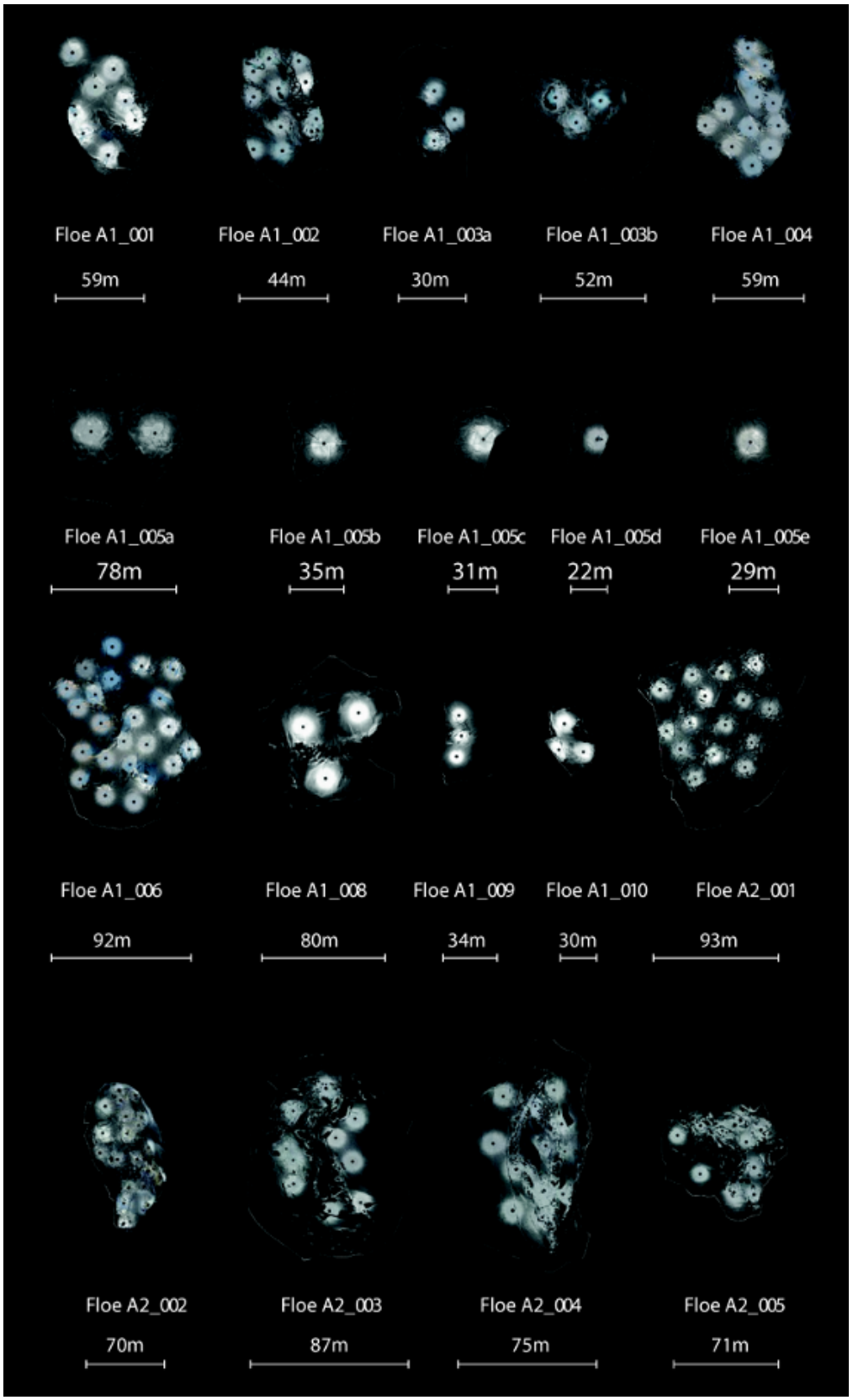

Figure 9: Overview of all ice floes scanned using 3D LiDAR technology during the SIDARUS-1 and SIDARUS-2 campaigns.

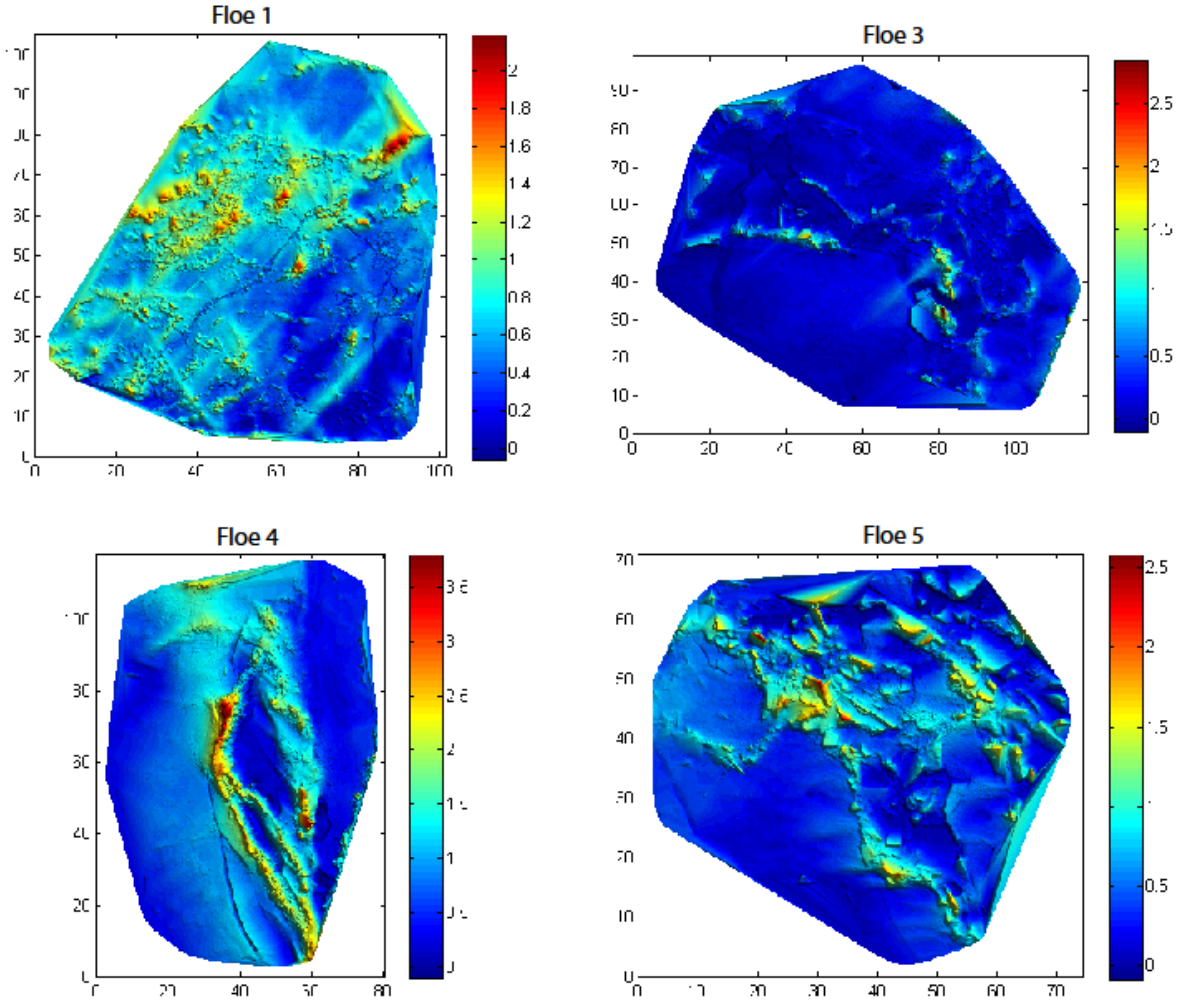

Figure 10: LiDAR data from floes 1, 3, 4 and 5 of AS12. The x and y axes are in metres. The z axis and colour bar represent freeboard in metres.

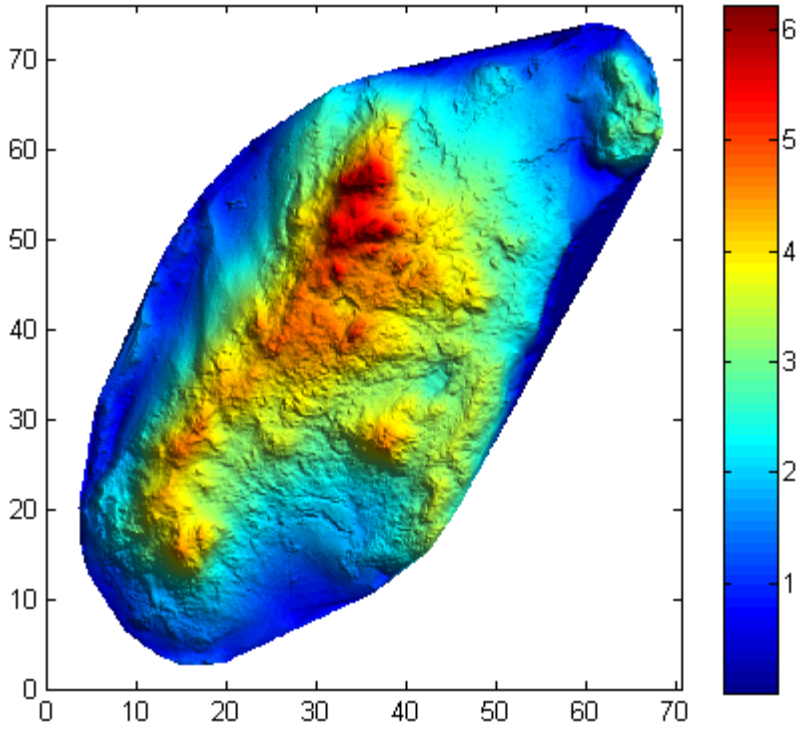

Figure 11: LiDAR data from floe 2 of AS12. The x and y axes are in metres. The z axis and colour bar represent freeboard in metres.

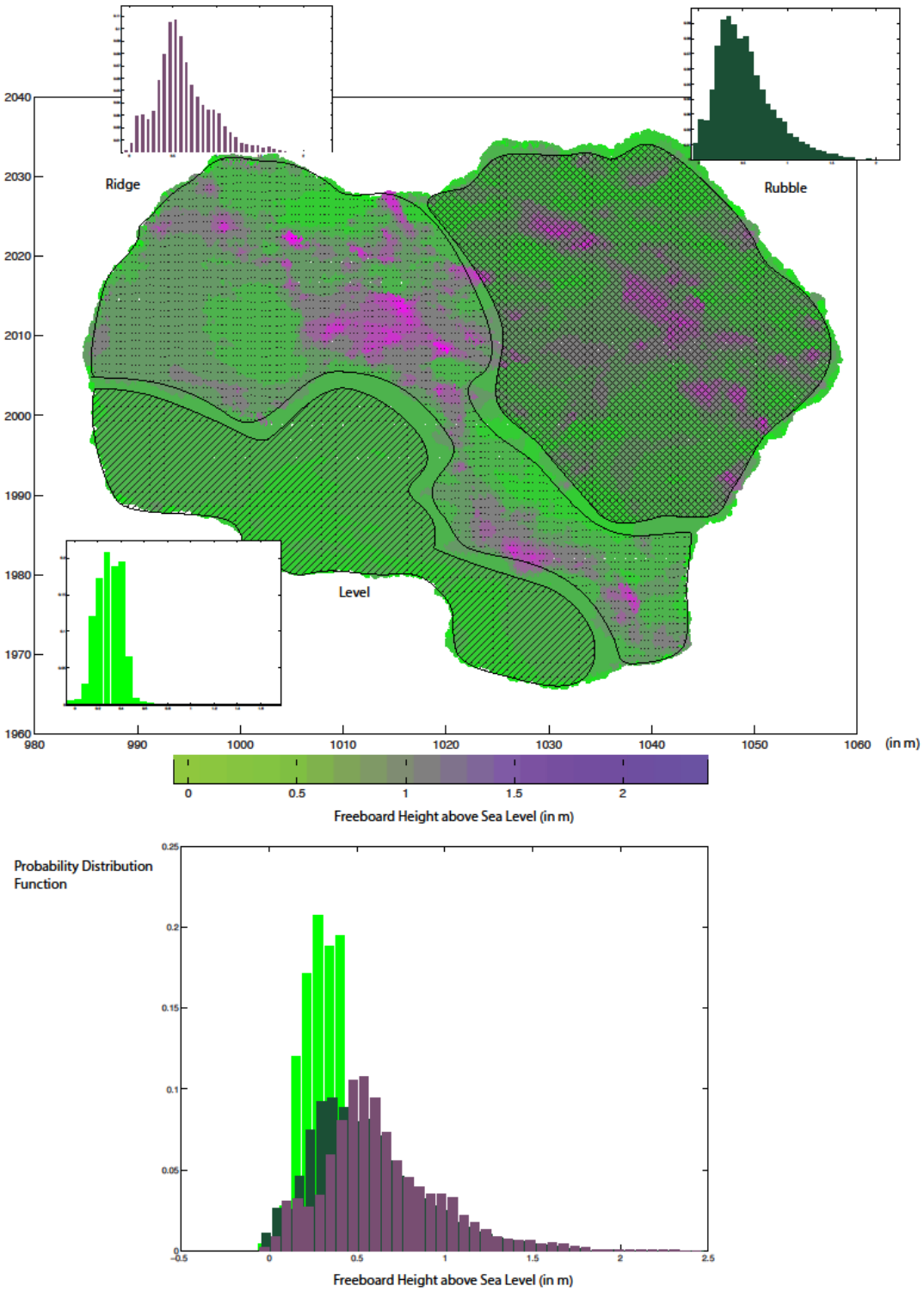

Figure 12: LiDAR scan of surface structure of floe 5 from AS12. Visually distinguishing three types of ice morphology (level, ridged, rubble) and probability density functions for the freeboard of for all three.

3.3 Drill lines

To obtain a comprehensive idea of the whole structure of the ice floe it is necessary to not only

measure its surface but also the snow cover and thickness in greatest possible detail. The different data sets (scans, snow and thickness) can then be tied together by means of a survey station, a typical output of which is seen on the right. As September is at the end of the melt season, there is rarely significant snow found on sea ice in the Arctic. The measured ice thicknesses varied greatly depending on whether the floe consisted of first year ice or multiyear ice. For first year ice, average thicknesses were usually around 1-2 m, whereas the older, more deformed, multiyear ice featured average thicknesses up to 4 m.

Scatter plots relating floe thickness and freeboard measurements are shown in figure 13 (for AS11) and figure 14 (for AS12). A positive correlation between freeboard and thickness was found in both cases. Figure 15 illustrates a compilation of the draft, freeboard and snow measurements for one drill line. Similar figures are included in the appendix, showing freeboard and draft profiles for all the drill lines taken in AS11.

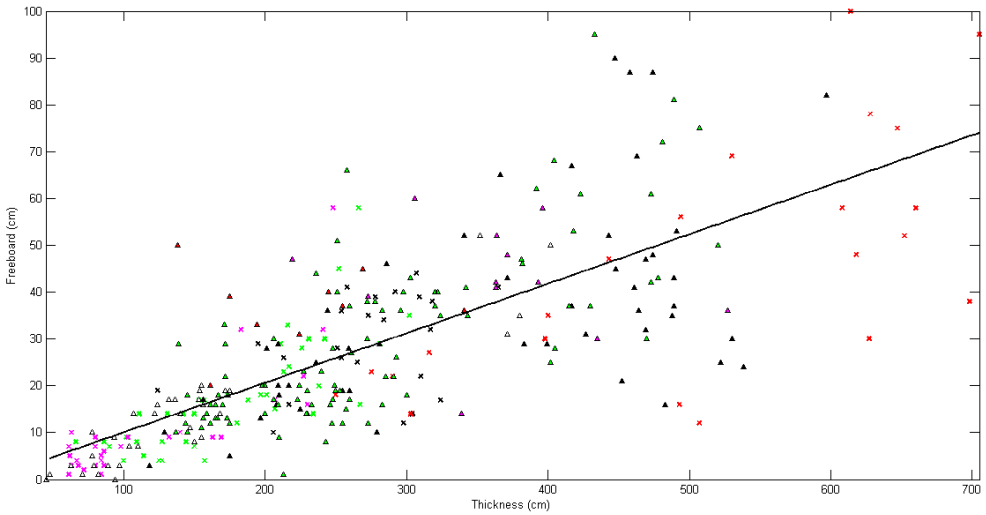

Figure 13: Scatter plot of floe freeboard vs. thickness for AS11 campaign. Each marker represents one of 9 different floes. There are 347 data points in total. Y-intercept: -0.5018 cm, slope: 0.1058, correlation coefficient: 0.7535.

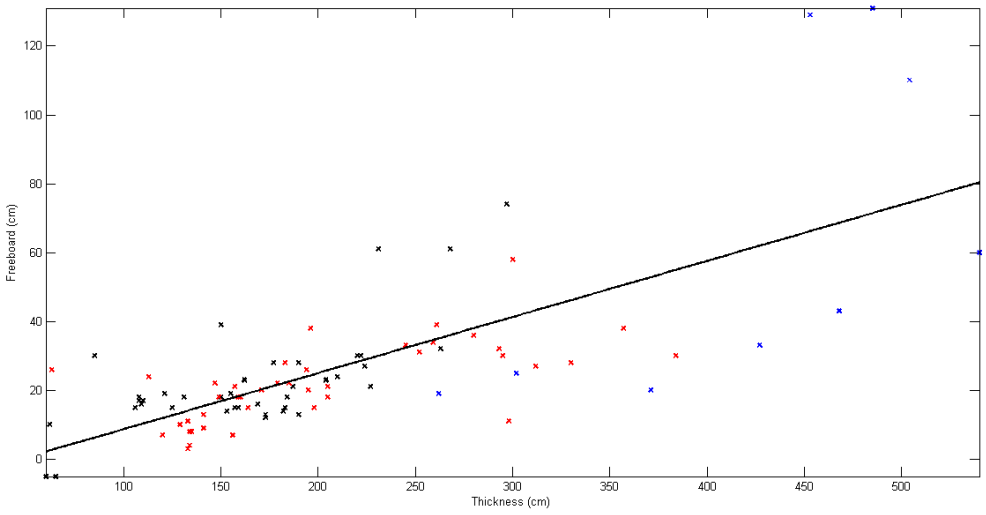

Figure 14: Scatter plot of floe freeboard vs. thickness for AS12 campaign. Each marker represents one

of 3 different floes. There are 89 data points in total. Y-intercept: -7.6078 cm, slope: 0.1629, correlation coefficient: 0.7267.

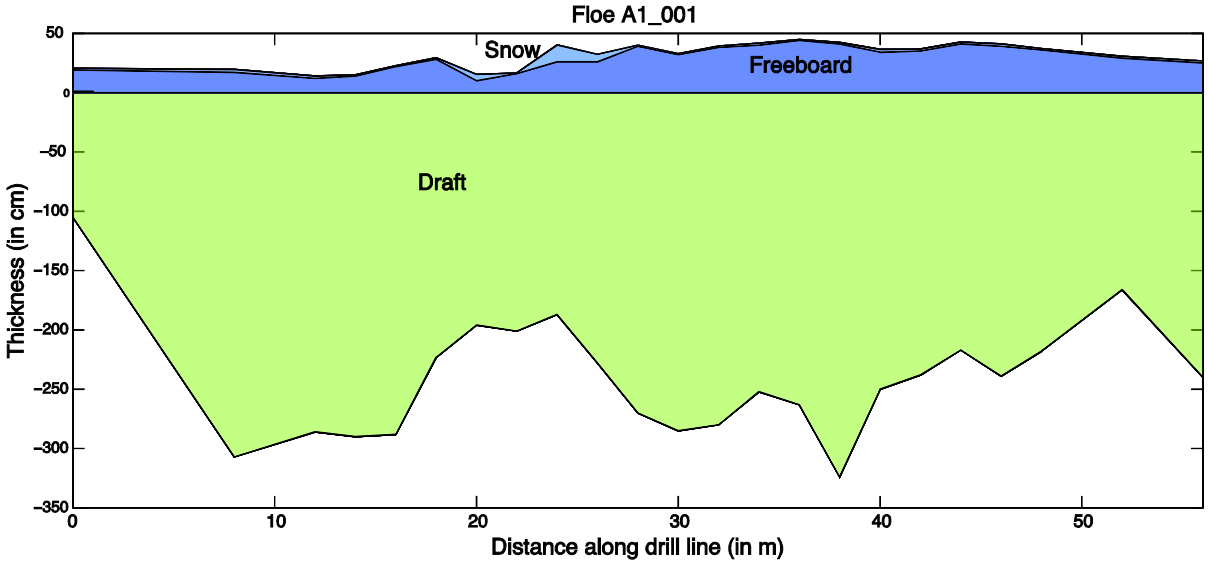

Figure 15: Example of a drill line plus snow depth measurements.

3.4 Aerial imaging

Grids and line patterns were own by the helicopter, enabling large scale aerial imagery surveying of the conditions in the local MIZ (survey areas: 1 - 50 nm^2). This will allow us to extract statistics like floe sizes (as function of distance to ice edge), preferred break up orientation, ridge frequencies and directions. The aerial photographs collected play an important role in providing a mesoscale that links the small scale results gained from studying individual floes to the basin wide surveys performed by satellite data. Comparing floe scans to aerial grids for example gives insights into how local ridge conditions affect the floe distribution over a larger area. This in turn provides information as to how to interpret data with much bigger footprints from satellite radars.

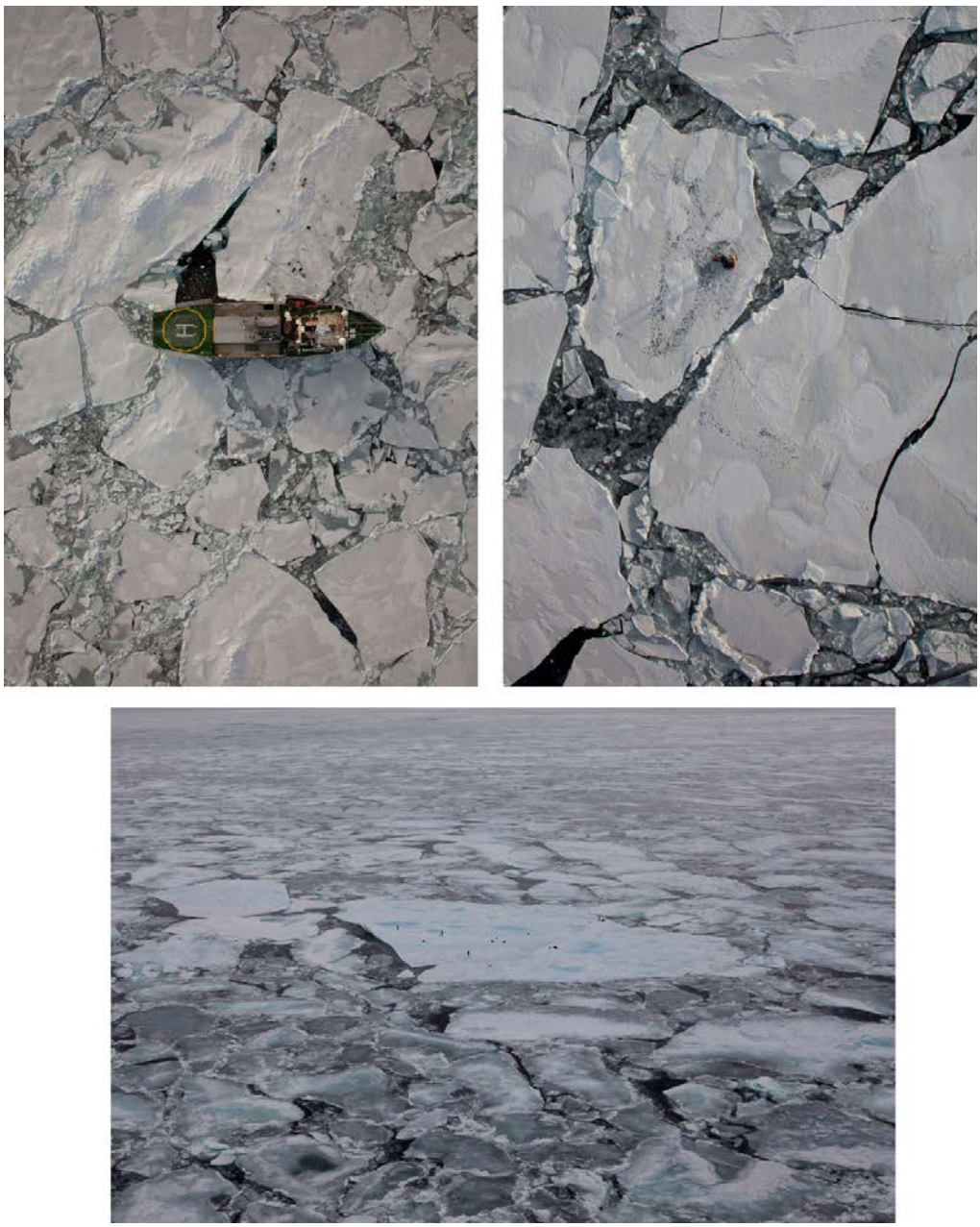

Figure 16: Aerial images of three of the floes surveyed during AS11 (clockwise from top left): A1_002; floes A1_005d (with 3 scientists) and A1_005e (adjacent to 5d bottom right); floe A1_003a and A1_003b (before breakup); Photographs: Nick Cobbing/Greenpeace

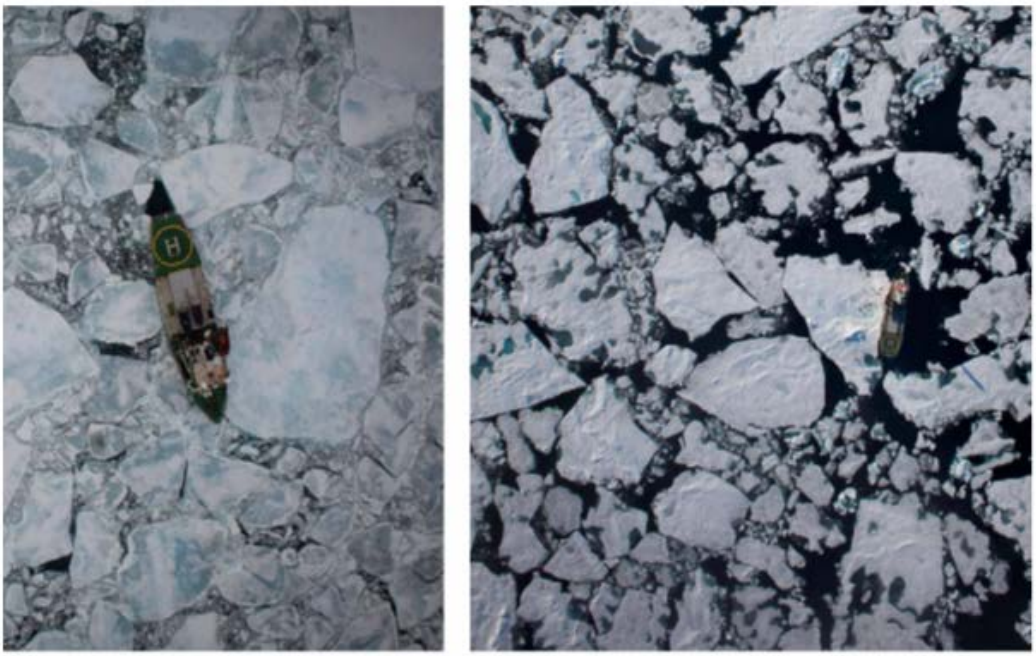

Figure 17: Aerial images of two of the floes surveyed during AS11: A1_004 (left); A1_001 (right); Photographs: Nick Cobbing/Greenpeace

Figure 18: Example aerial image obtained through AS11, the mosaicked image consists of 15 individual images (for scale the Arctic Sunrise can be seen in the center of the image).

Chapter 4: Discussion

4.1 AUV

The multibeam sonar data from the AUV suffered from two major issues. The first was the incomplete coverage of the floes. This may have been due to currents which prevented the AUV from following its preferred course. This prevented a complete characterisation of the underside of floes 1 and 3 being performed. The second is the presence of "streaks" in the data. These streaks were largely smoothed out during the processing of the data, however they remain present in some sections even after smoothing. Balancing the amount of smoothing performed such that the noise was reduced, but also such that the shape of major features could be resolved lead to a radius of smoothing of approximately 0.5 m being used on the data.

The issues associated with the data from the AUV limits attempts to collocate and compare AUV and LiDAR data, with identifying and aligning subsurface features with surface features posing an ongoing challenge which we continue to work on. However, for the stamukha in floe 2 of AS12, adequate AUV coverage has allowed for collocation with LiDAR to be attempted. Figure 19 shows the results of this attempt, where the peak draft values recorded by the AUV were aligned with the peak freeboard values from the LiDAR data.

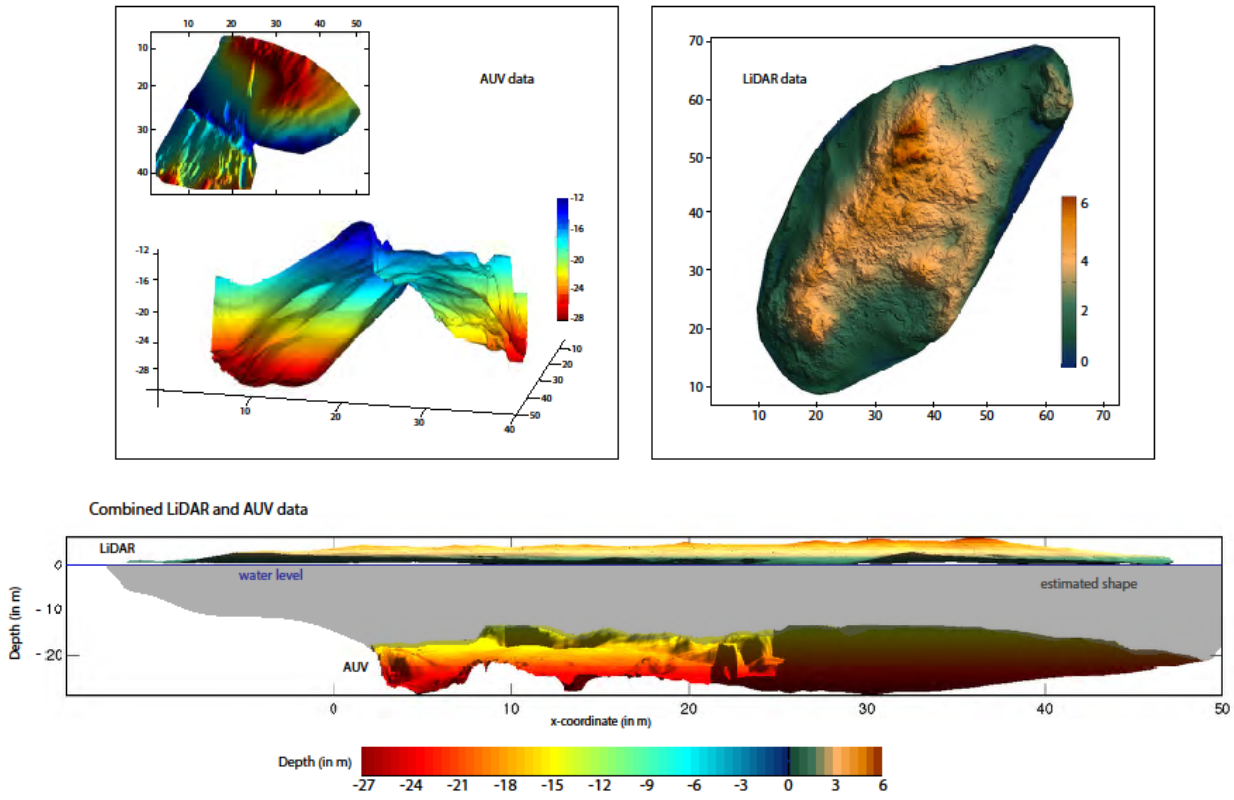

Figure 19: Collocated AUV and LiDAR data for the stamukha in floe 2 of AS12.

4.2 LiDAR

Probability density functions were generated for the data from floes 1-4 of AS12. The shapes of these PDFs reflect the morphology of the ice in each floe. For example, the more deformed floes from figures 10 and 11 (floe 1 and 2) are clearly distinguishable from the less deformed floe (3) by their wider spread of values and higher averages. For figure 4, two distinct floes are identifiable by the separate peaks in the PDF, suggesting a combination of more and less deformed ice.

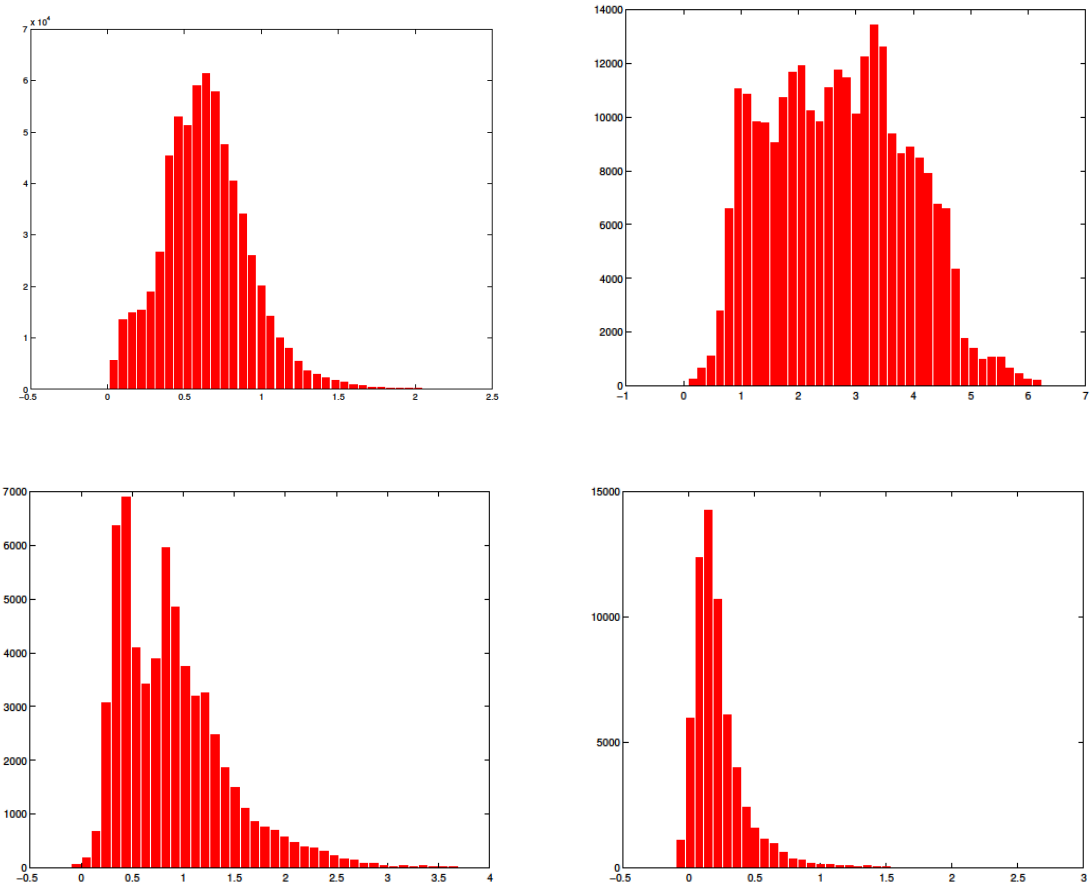

Figure 20: PDFs of LiDAR scans of surface structure of AS12 floes 1 to 4- see figures 10 and 11. Note the clearly distinguishable PDF shapes for different types of ice (clockwise from top left): multi-year `rubble' ice, smoothed PDF with freeboard up to 2 m; top hat shaped PDF for the Stamukha, representing the constant gradient of the conically shaped surface; narrow PDF for a level first year ice floe; two-peaked PDF for two floes of different thickness rafted - compare the surface plots of figure 8.

4.3 Drill data

The observed relationships between ice freeboard and thickness values for AS11 and AS12 are shown in figures 13 and 14. Least squares regression lines for these data were calculated, the slope of which suggests the following relationships between ice freeboard and thickness:

AS11: F = 0.1058 x H

AS12: F = 0.1629 x H

, where F is the freeboard elevation, H is the ice thickness and, assuming isostatic equilibrium, 0.1058 and 0.1629 are equal to:

$$1 - \frac{\rho_{ice}}{\rho_{water}}$$

The high correlation coefficients for the data, combined with a y intercepts close to zero, support the validity of this relationships. The slope values for this relationship are in good agreement with other similar estimates (0.106 from Alexandrov et al., 2010 and 0.111 from Wadhams 1992, 2000). The average density of the sea ice estimated from these relationships are 918 kg m^{-3} for AS11 and 860 kg m^{-3} for AS12, which are within the range of measured densities reported in the literature (e.g. 750 to 960 kg m^{-3} for first year and 720 to 940 kg m^{-3} for multiyear ice, Timco and Frederking, 1996).

From the above relationship, it can be inferred that the greater the slope, the lower the density of the ice relative to the water. Variations in the slope value could therefore be used as a proxy for differentiating ice regimes, as multiyear ice is generally of lower density as a result of fewer voids and lower salinity, therefore resulting in greater slopes. This has also been suggested by Ackley et al. (1974) who stated that higher freeboards lead to lower average densities after work on ice profiles on AIDJEX stations.

Floes 1, 2, 3, 6, 9, 10 and line 7D were identified as being deformed floes, while lines B-E for floe 5 and lines A-C for floe 7 were identified as being undeformed floes. The observed relationship between freeboard and thickness for deformed and undeformed floes is shown in figure 21. Counter to what would be expected, a greater slope was observed for undeformed floes than deformed floes. A number of possible explanations exist for this. Firstly, while multiyear ice is generally of a lower density than first year ice, large variations in the densities of both types of floe have been observed and the results may be unrepresentative of these floe types in general. There is also the possibility that differences in snow cover over both floe types may influence the freeboard to thickness relationships. It is also likely that pointwise isostatic equilibrium is not a reliable assumption, which combined with a possible systematic bias introduced by not drilling directly through the sails of the floes could explain the unexpected results.

It is also worth mentioning that the data does not appear to show distinct cut-offs between deformed and undeformed floes. Instead, the data imply more of a continuum of deformity.

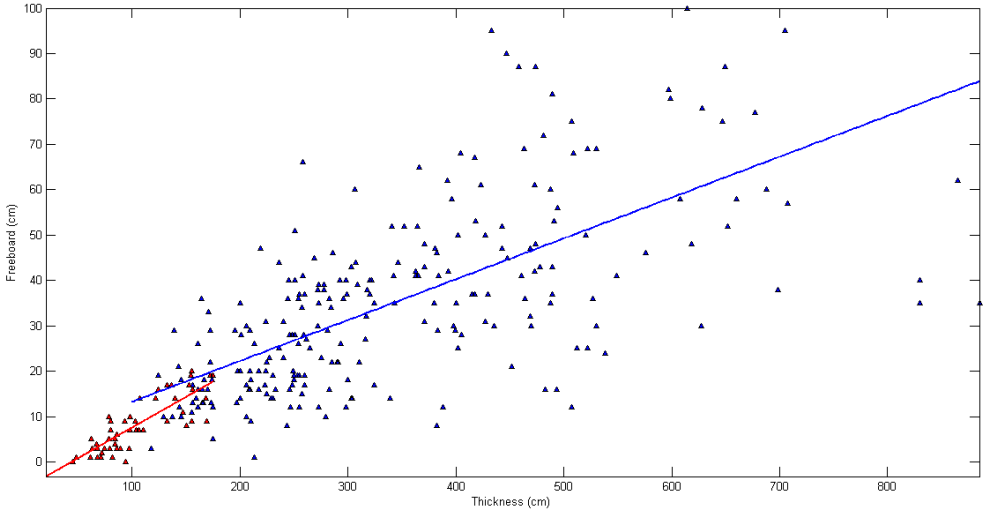

Figure 21: Scatter plot of floe freeboard vs. thickness for AS11 campaign. Blue triangles represent data from deformed floes and red triangles represent data from undeformed floes. There are 351 data points for deformed floes and 53 data points for undeformed floes.

For deformed floes: Y-intercept: 4.2740 cm, slope: 0.0900, correlation coefficient: 0.6561.

For undeformed floes: Y-intercept: -5.8763 cm, slope: 0.1348, correlation coefficient: 0.8299.

PART II: MAPPING OF ICE THICKNESS AND PRESSURE RIDGE SHAPES IN THE BEAUFORT SEA IN SUMMER 2014

Chapter 1: Introduction and Purpose of Work

The purpose of the 2014 AUV experiment was to map the three-dimensional structure of ice floes, and especially pressure ridges, in the melt zone of the Beaufort Sea in August. August is the month of most rapid retreat, preceding the mid-September ice minimum, and it is important to determine the main mechanisms governing the rate of retreat – for instance, whether it is ice dynamics, ice melt (disappearance of ice *in situ*), or the action of waves on the ice causing breakup and decay. It is also important to map the two main components of the ice cover – undeformed ice and ridged ice – in this season of rapid retreat, again to determine whether the undeformed ice is thinning rapidly and is the main source of the ice loss, and whether pressure ridges retain their shape and structural integrity through the decay process.

These aims can best be achieved by the use of upward-looking multibeam sonar from an autonomous underwater vehicle (AUV). It has been found in a number of field trials (Wadhams et al., 2004; Doble et al., 2009, 2011; Wadhams, 2009; Wadhams and Doble, 2008; Wadhams et al., 2008) that a small AUV launched from a ship or a slot cut in the ice can efficiently survey a pressure ridge and its environment by generating a mosaic of tracks each producing an image swath of 30-60 m width. From this we can derive:

1. the shape of the ice underside, particularly the slope angles and block texture of first-year and multi-year pressure ridges., but also the shape of an underside of undeformed ice where the upper surface is covered by a matrix of melt pools. Hence, by comparison with winter data (including data from the same area obtained in April 2007, Wadhams et al., 2008), we can understand the way in which summer decay processes work on the structure of the ridge.
2. with simultaneous data on top surface elevation, derived from the quadcopter, the relationship between freeboard and draft, testing the equivalent density of the ice in ridges ands producing values to be used in algorithms to interpret radar altimeter data.
3. applied quantities such as the oil containment potential (Wilkinson et al., 2007), given by injecting oil at random points on the mosaicked underside surface, and analysing the area of spread related to volume added, for a random collection of spots.

Chapter 2: Framework of Expedition Involved

In 2014 the AUV team was invited to take part in the “Arctic Shield 2014” programme by the United States Coast Guard. This employed the icebreaker USCGC “Healy” and took place from 8 to 24 August 2014 in the Beaufort Sea. The main purpose of Arctic Shield, building on similar exercises in 2012 and 2013, was to test the co-ordinated use of instruments and equipment which could be of use in the event of a major oil spill or blowout in US Arctic waters, when “Healy” would be the vessel taking formal responsibility for command and control in the response process. The AUV was therefore seen as a component in oil spill simulation testing as well as sub-ice profiling, and so the work assisted in the aims of WP4 of ACCESS as well as WP1. Lead agency on board was the US Coastguard Research and Development Branch in New London, Connecticut, with R Hansen as Chief Scientist.

We were assigned four berths which enabled the main AUV team to take part: P Wadhams (leader and relevant ACCESS partner); Bo Krogh (transponders and tracking; technical logistics); Richard Yeo (Gavia AUV expert and operator); plus one berth for the top surface mapping to match the underside maps. In the Fram Strait study in Part 1 we employed the services of Laser Scan Ltd. to conduct laser scanning surveys over the ice surface of the ridge being profiled by the AUV, but this requires a staff of two and only one berth was available, so we decided to test the ability of precision photogrammetry from an unmanned quadcopter to carry out the surface truth. Stephan Moelvig from COWI ApS therefore took part, bringing such a vehicle.

Other work to be carried out from the ship included a simulated oil spill in ice and testing of unmanned drone aircraft and aerostats for surface spill detection. Our work had to fit into this framework and there were surprising and unexpected limitations on the number of deployments that we were allowed to undertake, set by availability of boat crews to operate away from the ship.

Chapter 3: Description of Equipment

3.1 The Gavia AUV

The Gavia AUV is a compact lightweight AUV designed for manual deployment from ships and boats. We ourselves used it in ice surveys (Wadhams et al. 2007; Doble et al. 2009). In both cases it was deployed through a slot cut in the floor of a heated tent and operated with a Kevlar line both for insurance purposes and to ensure control in the event that the vehicle ignored its programmed instructions.

3.2 USBL transponder tracking system

The USBL transponder tracking system consists of:

1. A spar buoy with
2. The USBL Transducer (EvoLogics S2CR 18/34 USBL Head)
3. A GPS (Hemisphere V103 GPS/Glonass and heading)
4. A transponder/modem mounted on the AUV (EvoLogics S2CR 18/34 WiSE)

The 18/34 USBL (Ultra Short Base Line – measuring principle for the unit) is a simultaneous underwater positioning and communications system providing accurate 3D positioning and reliable data transmission.

The USBL has a horizontally omnidirectional beam pattern, optimized for medium range operations in reverberant shallow waters, such as under ice, and providing 3D positioning with a slant range accuracy of 0.01m and angular accuracy of 0.1 degrees.

The only USBL head available for this field work was a unit with an ethernet connection, and not a serial link. This meant that there had to be a cable connecting the USCGC Healy and the buoy.

Since the AUV, during two of the three successful under ice mapping experiments, operated more than 2 kilometres away from Healy with several ice floes and ridges in between, it meant that tracking only

was successful during one of these missions.

During the successful experiment it was shown that the AUV Positioning Buoy was able to accurately track the AUV.

Figure 3.1. Photograph of the tracking buoy, ready for deployment. Two people are necessary for this task.

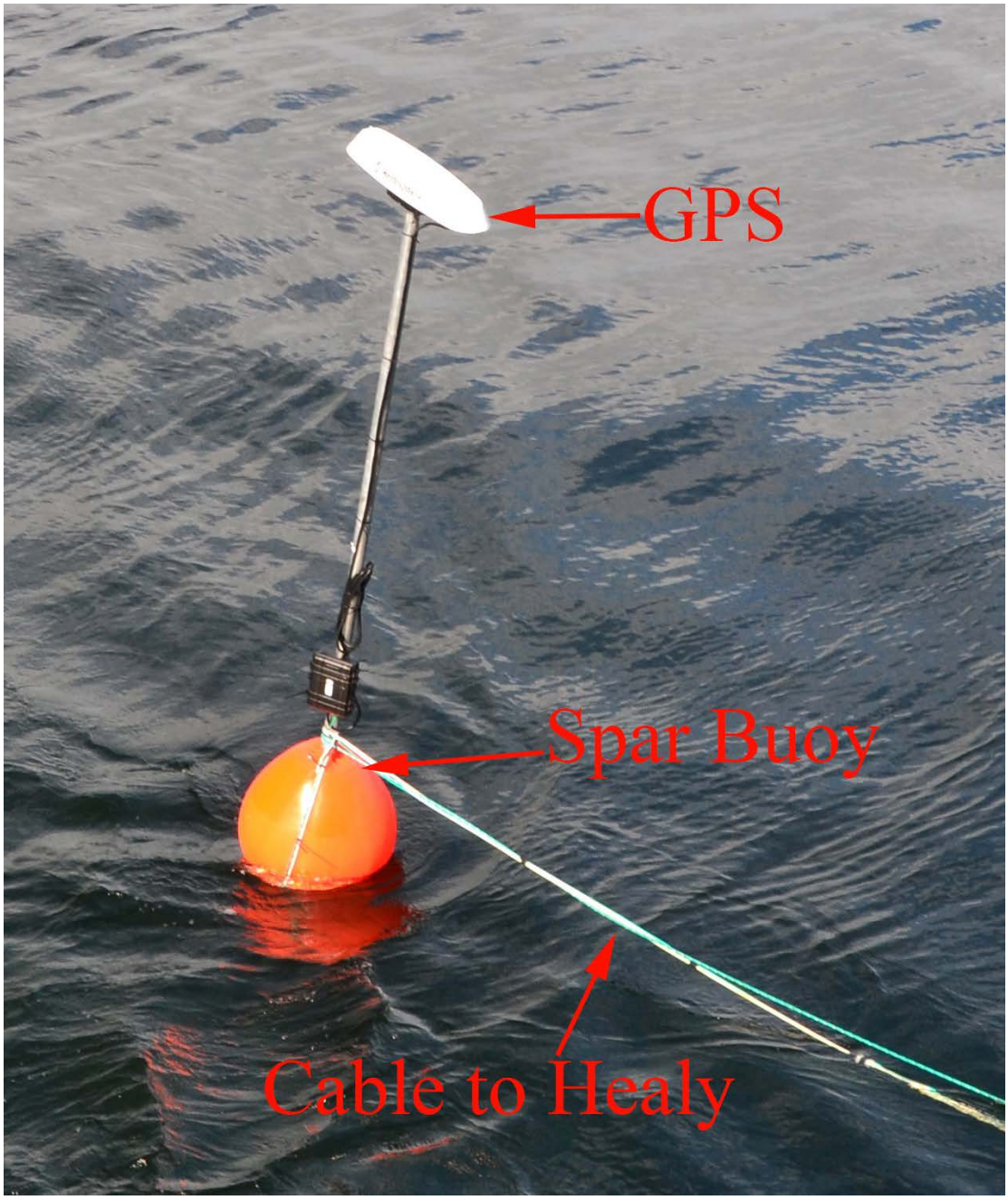

Figure 3.2. Tracking buoy in water.

3.3 Quadcopter

The Quadcopter, shown in Fig3.3, was supplied by Cowi A/S, a leading Danish consulting engineers company.

The Quadcopter, X8, is driven by 8 motors with propellers and powered by 2 lithium (4-cells) batteries each 10 Ah. The batteries are in an aluminium housing, and are thus puncture safe. The frame weighs 2.5 kg and is made of carbon parts. The gimbal weighs 1.4 kg (including sensor). The maximum take-off weight is 5 kg. The main electronics board, servos, gyro and other electrical components are hidden inside the main hull. A small antenna and wind speed sensor is placed on the outside. The weight and shape of the UAV makes it able to hover in a fixed position in the air or slowly descend/ascend to/from higher altitudes. However, the maximum speed has been estimated to 110 km/h. Overall, there are no sharp edges except for the 8 propellers.

Figure 3.3. The Quadcopter.

Unfortunately, the quadcopter could not be used. There wasn't FAA approval to launch the quadcopter from the helideck and the ice was too rotten to be able to launch the quadcopter from the ice.
The purpose of bringing a Quadcopter was that it should have been launched simultaneously with the AUV and surveyed the same ice floes from above, thus enabling the processing of the two datasets into a 3D model of the ice.

Chapter 4: Mobilisation for voyage

The AUV operation in 2014 involved the use of a Gavia AUV rented from the University of Iceland, which was broken down into a series of boxes and sent to Seward, Alaska, to meet the USCG "Healy". The scientists involved in the cruise mobilised via Reykjavik, Iceland. This comprised Bo Krogh (from Denmark), Dr Richard Yeo (from Reykjavik), Stephan Moelvig (from Copenhagen via Reykjavik) and Prof Peter Wadhams (from London via Reykjavik). After arrival in Anchorage via Icelandair from Reykjavik, the group of 4 rented a truck and drove the equipment to Seward, Alaska, to meet the "Healy". Further efforts were made to locate and retrieve equipment sent earlier to Seaward. All personnel and equipment were successfully assembled by sailing day.

Chapter 5: Description of Operations

5.1 Voyage from Seward to Beaufort Sea

USCGC "Healy" sailed from Seward on August 8 2014, passed down Resurrection Bay and entered the North Pacific. The track is shown in Figure 5.1. The ship passed through Shelikof Strait between the mainland and Kodiak Island. Unimak Pass was transited on August 10 and the ship proceeded northwards through the Bering Sea. On August 11 the AUV and transponder unit were tested in the water with the ship west of Nunivat Island. The ship moored off Nome on August 12 and carried out a further open water test of the Gavia AUV. An unusual characteristic of the environment was the extremely warm sea surface temperature (SST), mapped by an along-track sensor. This was later retrieved from the along-track record and is shown in Figure 5.2.

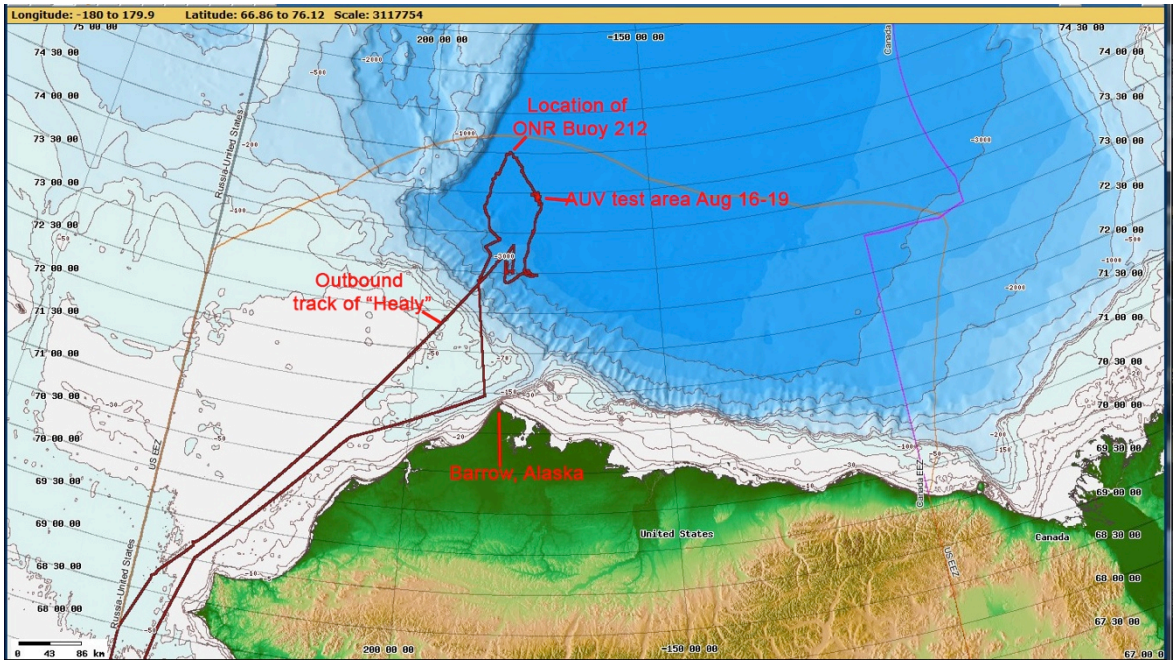

Figure 5.1. Map of Alaska, the Chuckchi Sea and the Beaufort Sea with the track of the USCGC Healy.

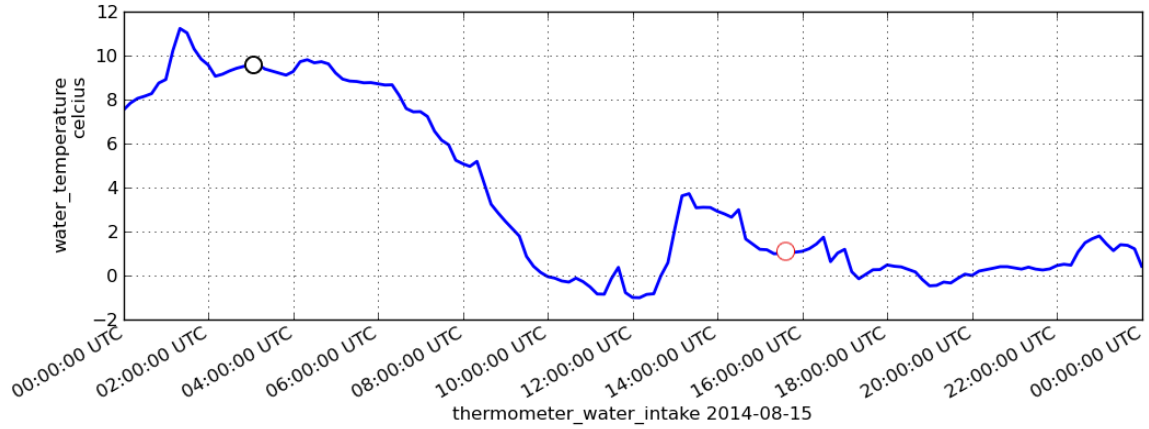

Figure 5.2. Along-track sea surface temperature record (sensor at 5 m depth). The red circle indicates the location of the ice edge.

The ship sailed from Nome on August 13, passed through Bering Strait during the night and entered the Chukchi Sea. The sea surface temperature started decreasing rapidly. Strong easterly winds (greater than 30 kts) were experienced, which lasted two days.

On August 15 the extreme ice edge was encountered, with appropriate warning given by the ice radar. The ice consisted of a wide band of broken up and rather rotted floes, with meltwater pools and lots of brash fragments. We sailed in, across the almost open water which lay behind, and up into the firmer denser ice of the main edge zone, with a gap in between about 1630 showing that the first concentrated ice was in fact a downwind band broken up by waves and wind.

5.2 Preliminary trials (Aug 16 and 17): results and problems

The first attempt at an AUV deployment was made on August 16, but no data were obtained because of a software problem. On the following day, August 17, a further attempt was made, but there were problems with the tether, and again no data were obtained.

Since the Gavia AUV was equipped with a standard downward looking GeoSwath MultiBeam Echosounder, it was ballasted so that, during operations, the whole AUV was turned up-side-down, so that the bathymetry of the underside of the ice was surveyed.

The problems with communications occurred when the AUV was inverted just prior to launching. The cause was probably a combination of cables moving during the inversion, and thermal contraction/stiffening of the connectors and cables when the system entered the cold water.

The first successful operation was on August 18.

5.3 First Experiment, August 18

August 18 was a perfect day with calm conditions for AUV operations. We were allowed to use the larger boat, the Arctic Survey Boat, shown in Figure 5.3.

Initially there were some issues with line handling as the line came off the spool, which caused aborts when the line became tangled during payout. This was solved on subsequent days by paying the line out into a large bucket before the missions, so it ran out smoothly.

There was some evidence of the problems that dogged later runs, where the Doppler Velocity Log (DVL) 'altimeter' (actually measuring distance to the underside of the ice from the AUV when inverted) reported intermittent false ranges, which caused the AUV to decrease its depth due to bottom avoidance behaviour inherent in the standard software. When running inverted under ice this behaviour can lead to the AUV attempting to surface under the floe.

During this experiment a dataset of 250 m by 250 m was obtained. Figure 5.4 shows the typical ice that was surveyed.

Figure 5.3. Launch of the Gavia AUV from the bow of the Arctic Survey Boat

Figure 5.4. The Arctic Survey Boat and the ice being surveyed.

5.4 Second and Third Experiment, August 19

August 19 was the most successful day of the voyage, where we were given two time-slots, from 1000-1200 and again from 1500-1730.

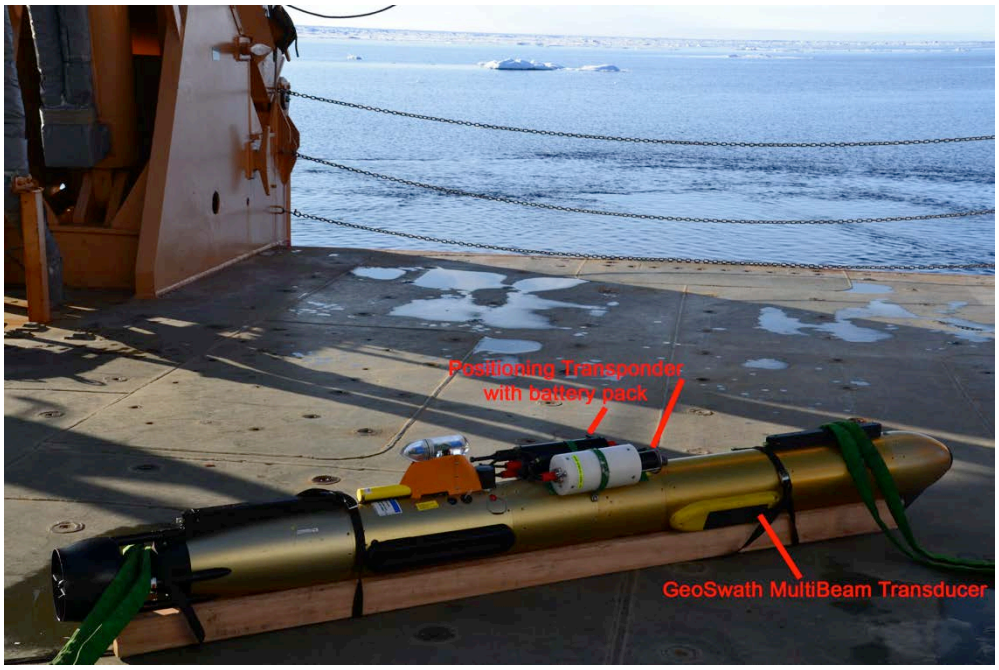

Figure 5.5. Gavia AUV aligning positioning system on back deck of "Healy" prior to launch.

During these further dives, further problems arose with false ranges from the DVL, resulting in the AUV failing to follow the depth set in the mission (15m in Figure 5.6). This in turn resulted in the poor data quality seen in 2014C, as the AUVs calculated position and sonar data were compromised by the continual pitch, velocity and depth variations.

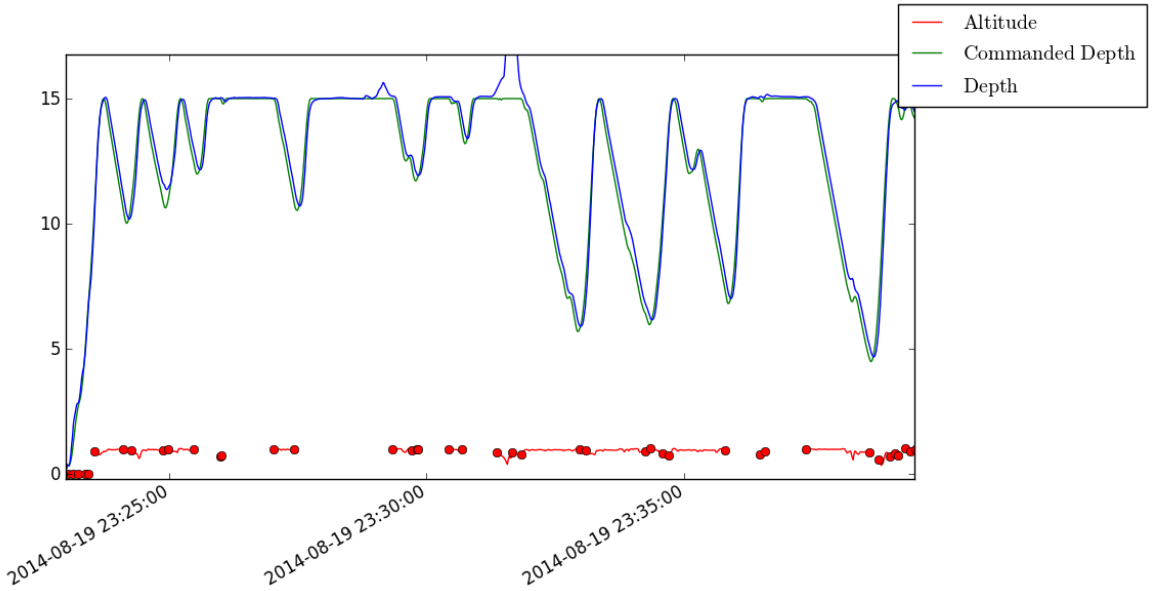

Figure 5.6. Depth of AUV. The AUV was set to follow a depth of 15m, but sometimes failed to achieve this.

Attempts were made to avoid these issues, and AUV data logs were sent to the manufacturers, but sadly no solution was made available. The cause of the false ranges was not entirely clear, and some missions ran without issues.

Two good datasets were obtained during these surveys. The AUV Positioning Buoy was also launched on both occasions, where the operations were carried out closer than 2 kilometers from the USCGC Healy, and thereby within range of the Buoy. The AUV was tracked successfully under the ice during the entire survey.

Figure 5.7. AUV Positioning Buoy as launched from the back deck of "Healy"

5.5 AUV Draft measurements

The AUV acquired data at four locations, shown in Figure 5.8. On each occasion ice draft data were collected, with good results on three of the four (2014A, B and D) deployments. The draft depths measured by the AUV are shown in Figures 5.9 to 5.13. At each site the data are shown both in plan with a colour scale consistent across all datasets. For the datasets with good results, the data are shown in perspective with a stretched depth axis and with a colour scale covering the local minimum and maximum. An upper cut-off was set for the draft values on some figures so as to remove anomalous data including measurements of the ship's hull.

Data from floe 2014A are shown in Figure 5.9. The floe appears to be mostly composed of either thin ice or open water. A number of small, block shaped features, likely to be partially melted ridges, interrupt this pattern. An artifact created by the ship's hull can be seen at 80 m N, 45 m E.

Data from floe 2014B are shown in Figure 5.10. There is some overlap between floe 2014A and 2014B, however as the datasets were not gathered at identical times, movement of the ice means that the same floe may not have been investigated. As in 2014A, the floe appears to be mostly composed of either thin ice or open water. A block with a draft of 6 m is present at 120 m N, 370 m E, deeper than those in 2014A. The blocks also include a large 2m deep feature centered at 200 m N, 100 m E. An artifact of the incomplete removal of the ship's hull from the data can be seen at 300 m N, 200 m E.

Data from floe 2014C are shown in Figure 5.11. As described above, the data acquired at this site were

of poor quality because of a malfunction in the AUV. There was no clear way to separate the anomalous data. An attempt was made to identify the free surface to get the correct drafts, but this still led to erroneous drafts with negative values. Here we show only data with drafts between -2 m and 7 m.

Data from floe 2014D are shown in Figures 5.12 and 5.13. A lower proportion of area of floe 2014D than floes 2014A and 2014B is composed of thin ice or open water, with deeper ridges and blocks covering a much greater proportion. These ridges show more linearity and a more coherent structure to the blocks than seen in the other floe, with one particularly large ridge crossing the whole way across the middle of the figures at 150 m N, 150 m E. A large, deep feature, or collection of blocks can also be seen to the North-East of the figures.

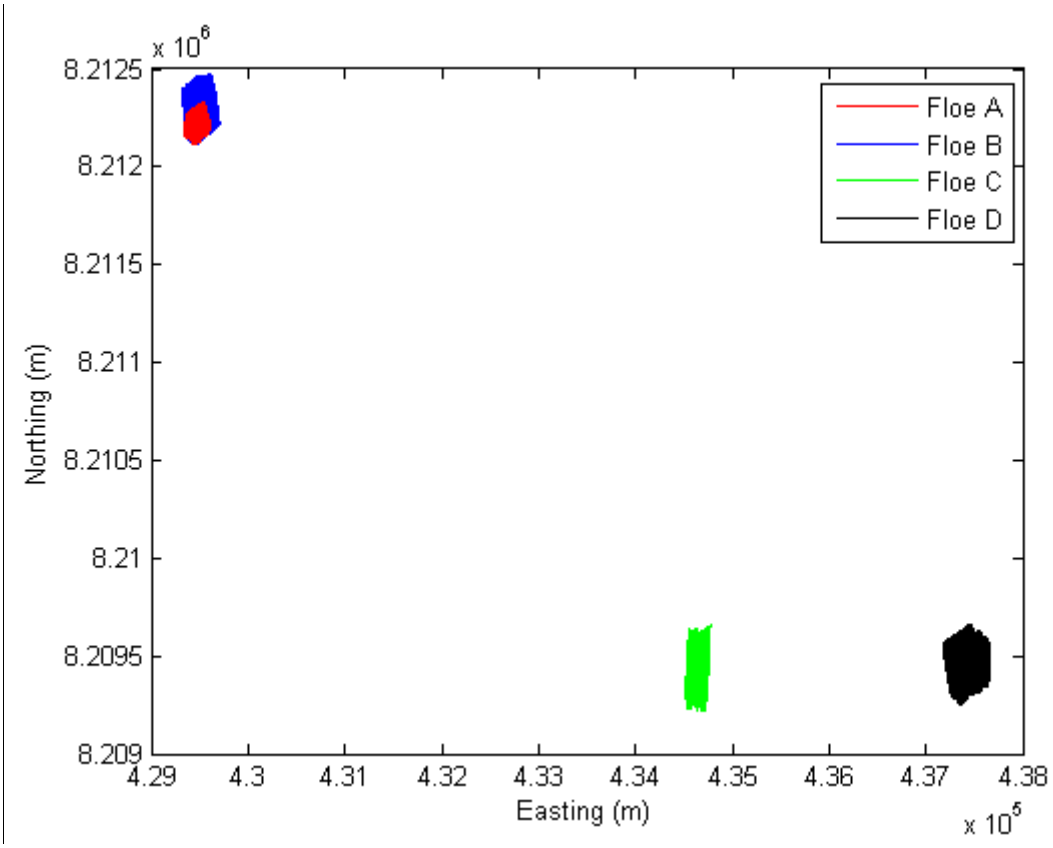

Figure 5.8. Map showing position of each floe (hereon referred to as 2014A to 2014D) in zone 5X in UTM coordinates.

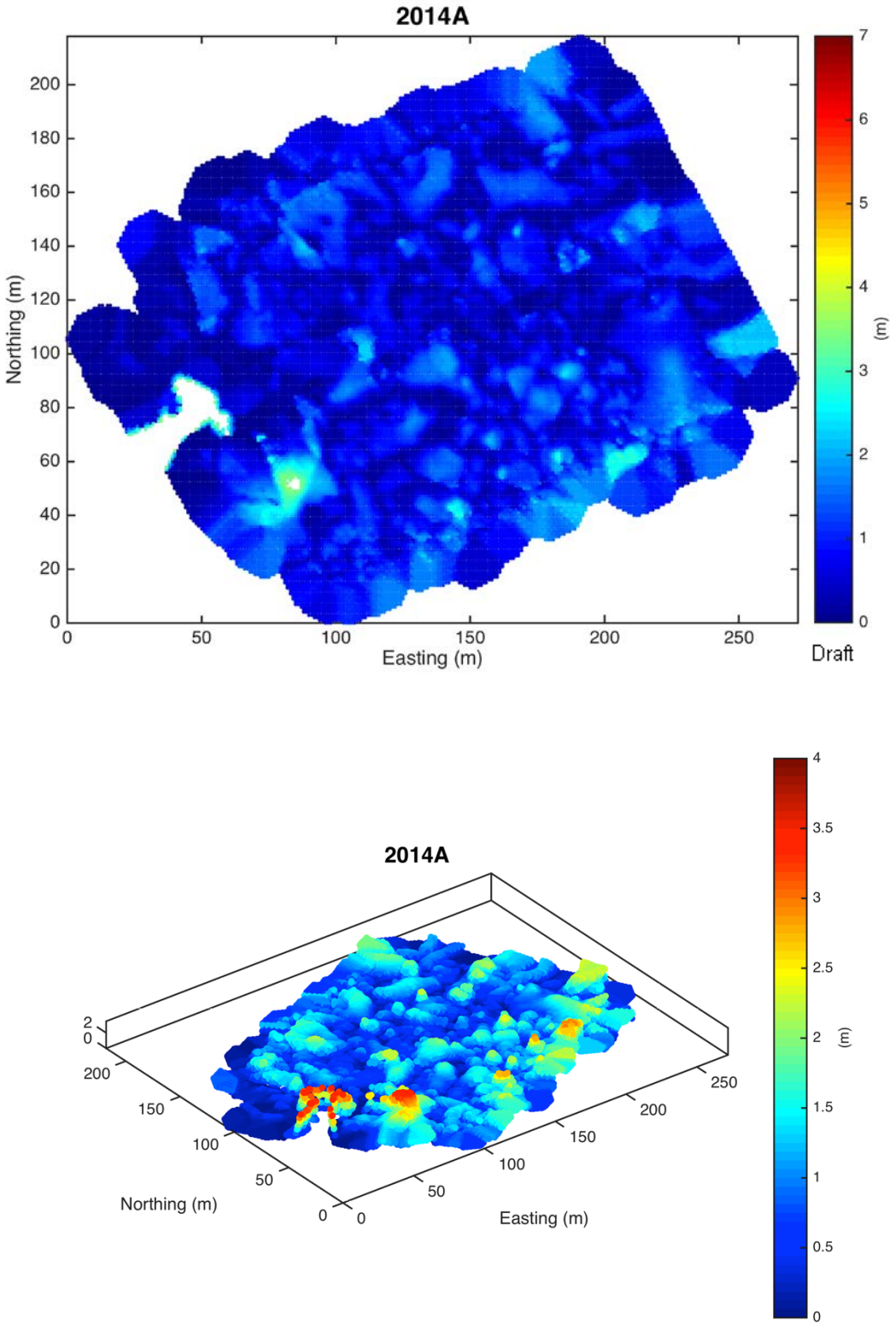

Figure 5.9. Draft measured by the AUV at floe 2014A.

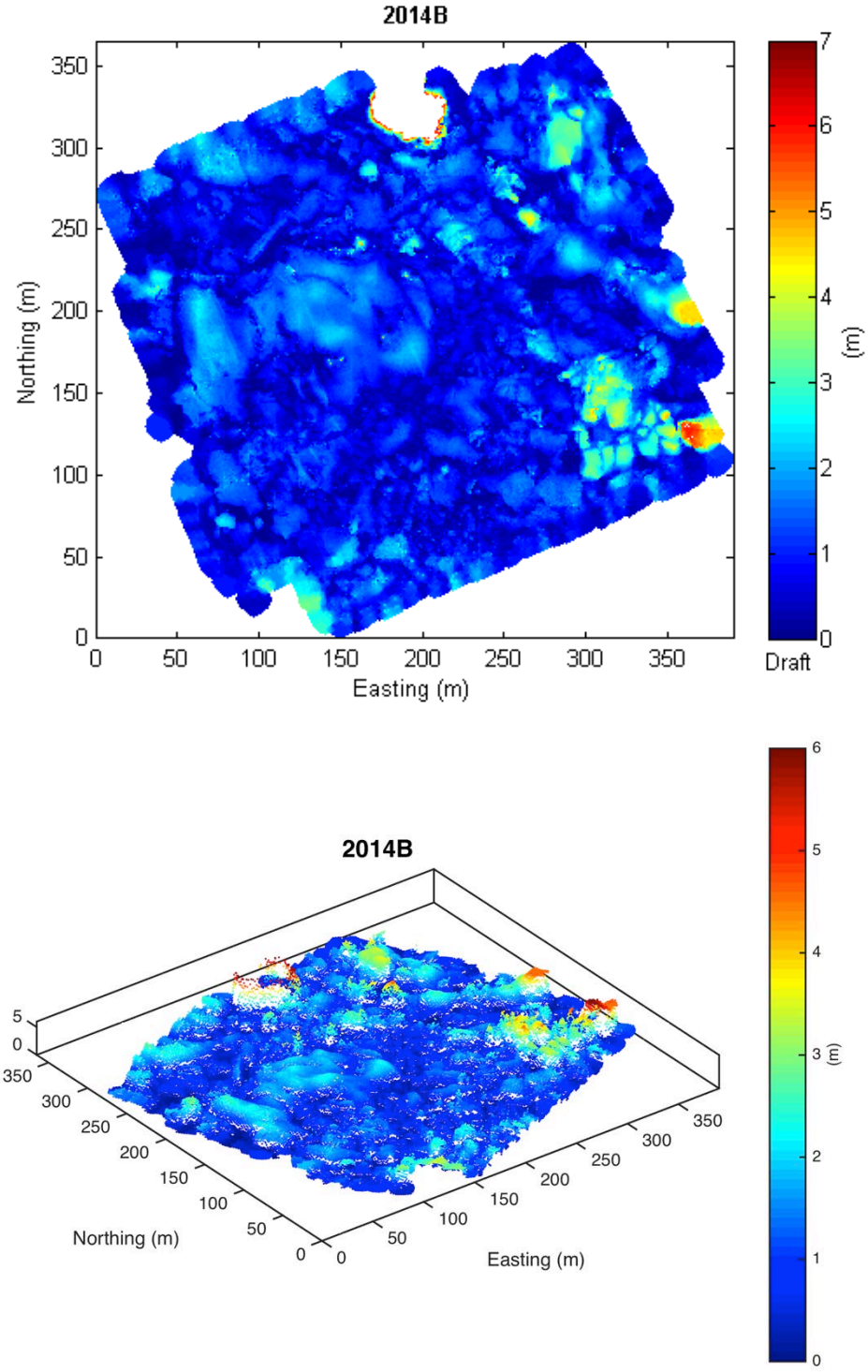

Figure 5.10. Draft measured by the AUV at floe 2014B.

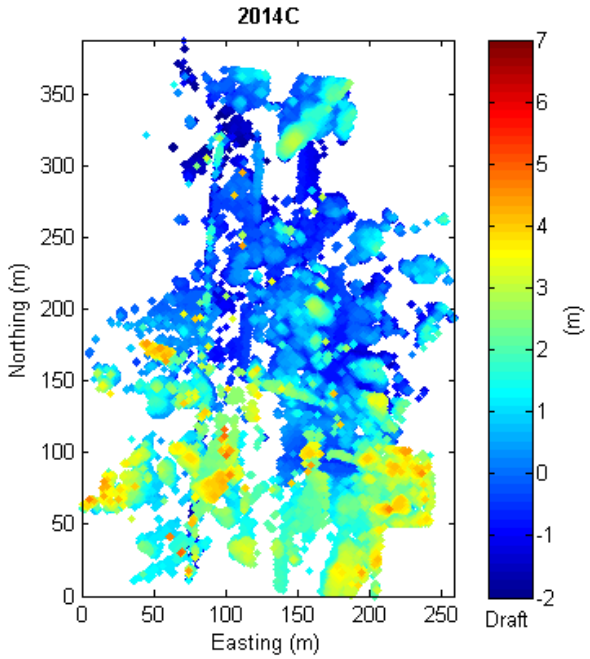

Figure 5.11. Draft measured by the AUV at floe 2014C. Problems with the DVL 'altimeter' led to poor data quality on this deployment.

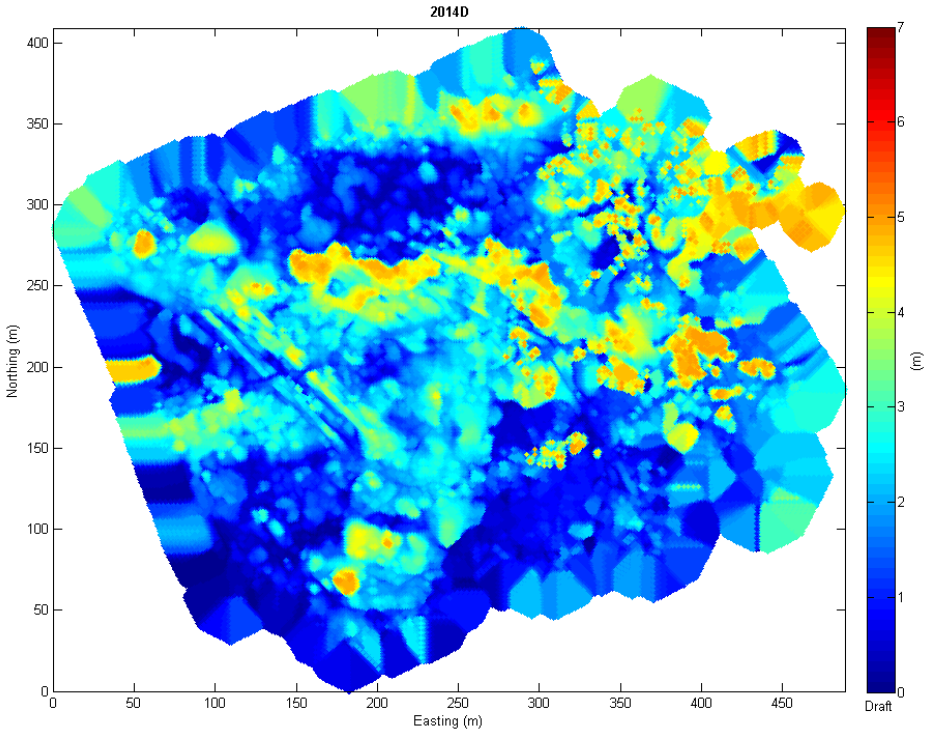

Figure 5.12. Draft measured by the AUV at floe 2014B without trimming edge of field. The data shown on the edges of the area recorded by the AUV appear to repeat, creating a misleading representation of the underside of the floe. A trimming process was performed manually to remove these repeated edge measurements.

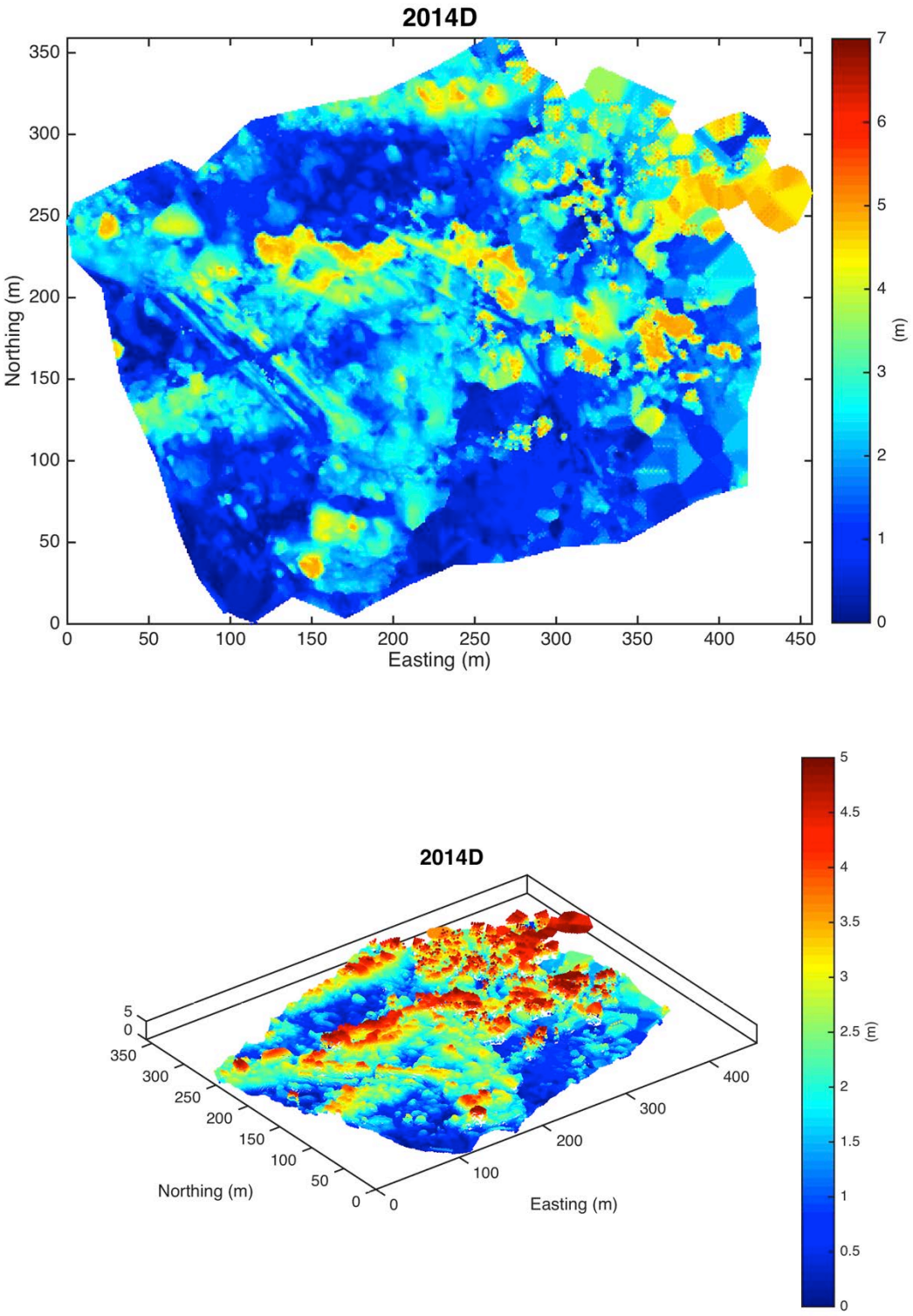

Figure 5.13. AUV data from floe 2014D. The data for these figures were manually trimmed to remove misleading repeat values around the edges.

5.3 Wave buoy interactions August 20

The opportunity arose to visit the site of one of the 30 wave-ice buoys deployed as part of the ONR MIZ programme to measure wave penetration and decay in the retreating marginal ice zone. The buoy was transmitting its position by Iridium.

At 12 the buoy appeared through poor visibility (Figure 5.13). It was a plastic dome on a black flotation collar with a stalk sticking down into a hole in the ice. It was sitting near the edge of a very rotted floe, was half out of its socket and lying half on its side.

Figure 5.13. Wave buoy 212 of ONR-MIZ programme.

Chapter 6: Results of mapping operations

The ice mapping operations during the voyage were restricted by operational restrictions characteristic of the Coastguard and the results were disappointing in terms of hoped-for measurement opportunities. Nevertheless, Gavia worked well during allowed deployments and obtained a series of very revealing mosaics of the under-ice surface at a time of extreme decay and rottenness of an ice cover which was about to disappear. Some preliminary conclusions that we can come to, especially in relation to the multi-year ridge profiles obtained in Fram Strait in 2012, are as follows:

1. All ridges were degraded and none retained full linearity. Where a prominent surface feature was observed and used as a target for AUV launch, there was a prominent submerged feature under it, but all ridges appeared to be broken up into individual blocks which were melting – in effect, the ridge was dissociating into its constituent parts and retained no strength.

2. The ridges did, however, retain significant volume with respect to the thin undeformed ice around it (typically 0.8 m thick or less). This indicates that, counter-intuitively, the final stages of ice decay in summer involve the pressure ridges acting as “ice volume reservoirs”, where a significant fraction of the remaining ice mass is concentrated. The ice in floes 2014A and 2014B had less ice mass and fewer large blocks than 2014D. One can envisage, of course, a slightly later stage of decay where the undeformed ice has gone and the ridge itself disintegrates into individual floating ice blocks which themselves then melt. We therefore view pressure ridges as having a delaying effect on the final ice disintegration process.

3. In a region like Fram Strait where the first-year ice is still robust and there are also multi year ridges (like the stamukha seen in 2012), ridged ice plays much more of the role that it plays during the winter, i.e. retaining a robust mechanical structure, and contributing towards the overall probability density function of thickness.

The most useful application of the 2014 data is therefore toward the development of an end-of-life model for a deformed ice cover undergoing terminal melt. This will be the subject of a forthcoming paper.

Chapter 7: Conclusions on properties and topography of melting ice

As described above, we conclude that in the early stages of summer melt a pressure ridge can retain much of its winter structure, especially if it is a multi-year ridge such as the stamukha and other ridges seen in Fram Strait in 2012. In fact the stamukha represents a class of ridge that has spent many complete summers aground on the continental shelf while the ice around it has disappeared and re-formed.

In the case of first-year ice, and at a more advanced stage of melt such as seen in August 2014 in the Beaufort Sea, ridges appear to break up into individual blocks and lose the coherence of their underwater structure (e.g. linearity disappears). However the ridges still represent a large, and possibly dominant, fraction of the remaining ice volume in the rotting ice cover, and as such can be seen as an ice reservoir.

Finally, what lessons do our field experiences have for the future of ice bottom mapping by short-range AUV? We can draw the following:

1. (From 2012) A slow-moving vehicle where depth control is achieved by vertical propeller (WHOI vehicle) is not suitable for use under ice floes in a marginal ice zone situation where shear currents may occur, as they are likely to be driven further under a floe and be incapable of following a programmed course outward.

2. A faster moving vehicle like Gavia is more appropriate as well as being easier to launch and recover.

3. The single short-baseline acoustic tracking system is potentially better than the multiple transducer system used by WHOI, because of quickness of deployment. Installing two or three transducers through the ice in 2012 meant that the floe of interest could break up in the time which it took to set up the system for the profiling operation. We feel that the future lies with single-buoy tracking systems.

4. There is always a trade-off between sophistication and cost. For instance, during earlier surveys we found Autosub to be a superb vehicle for under-ice use (Wadhams, P.**,** J.P. Wilkinson and S.D. McPhail. A new view of the underside of Arctic sea ice. *Geoophy. Res. Lett.*, **33**, L04501, doi:10.1029/2005GL025131). Yet it is very expensive, large and requires a large ship for deployment. There are systems even cheaper and more basic than Gavia, which possibly have the advantage that an under-ice loss would not be a major financial loss. Somewhere between these extremes an optimum solution remains to be found.

5. If an AUV-buoy-sonar system that works reliably at low cost can be identified for routine use, its use in combination with a surface mapping system (laser or photogrammetry) will be very valuable in improving our understanding of the critical processes of ice deformation and summer ice decay, as well as validation of airborne and satellite-borne altimetry systems.

We are aware that the data from these floes give us the ability to estimate the contribution made by deformed ice to the total ice budget at a time of extreme melt and disintegration immediately preceding complete loss of the ice. We are carrying out this calculation at the moment, adding data from other sources, and results will appear in a forthcoming issue of AMBIO.

References

Doble, M.J., A.L. Forrest, P**.** Wadhams and B.E. Laval (2009). Through-ice AUV deployment: operational and technical experience from two seasons of Arctic fieldwork. *Cold Regions Sci. Technol.*, **56**, 90-97

Doble, M J, H Skourup, P. Wadhams and C.A. Geiger (2011). The relation between Arctic sea ice surface elevation and draft: a case study using co-incident AUV sonar and airborne scanning laser. *J. Geophys. Res.*,**116,** C00E03, doi:10.1029/2011JC007076.

Wadhams, P., J.P. Wilkinson and A. Kaletzky (2004). Sidescan sonar imagery of the winter marginal ice zone obtained from an AUV. *J. Atmos. Oceanic Technol.*, **21**, 1462-1470.

Wadhams, P**.,** J.P. Wilkinson and M.J. Doble (2008). Three-dimensional mapping of the sea ice underside from AUVs and applications to the offshore industry. Proc. ICETECH 2008, Intl. Conf. on Performance of Ships and Structures in Ice, Banff, July 20-23 2008. Soc. Naval Archit. Marine Engrs, ISBN 978-0-9780896-1

Wadhams, P. (2009). The use of autonomous underwater vehicles to map the variability of under-ice topography. *Ocean Dynamics,* **62,** 439-447.

Wadhams, P. and M.J. Doble (2008). Digital terrain mapping of the underside of sea ice from a small AUV. *Geophys. Res. Lett.*, **35**, L01501, doi:10.1029/2007GL031921.

Wilkinson, J.P., P. Wadhams and N.E. Hughes (2007). Modelling the spread of oil under fast sea ice using three-dimensional multibeam sonar data. *Geophys. Res. Lett.*, **34**, L22506, doi:10.1029/2007GL031754.

Appendix: AS11 drill line profiles

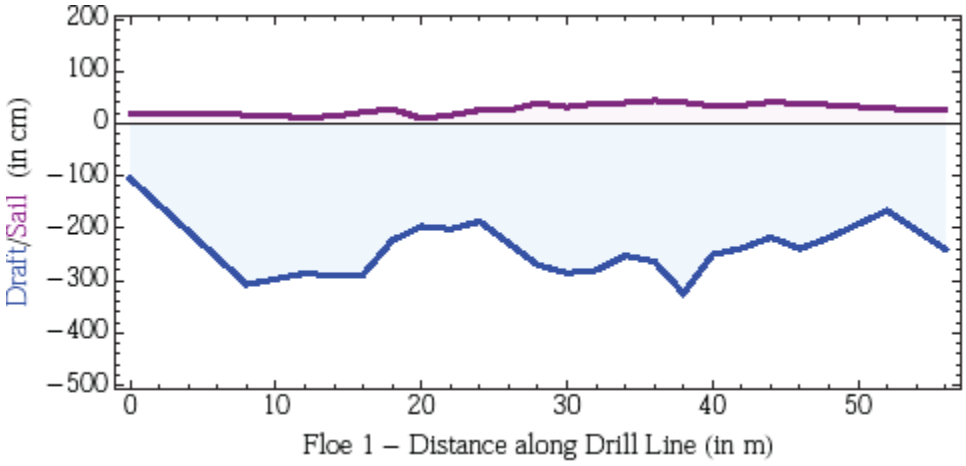

Floe 1 ALine

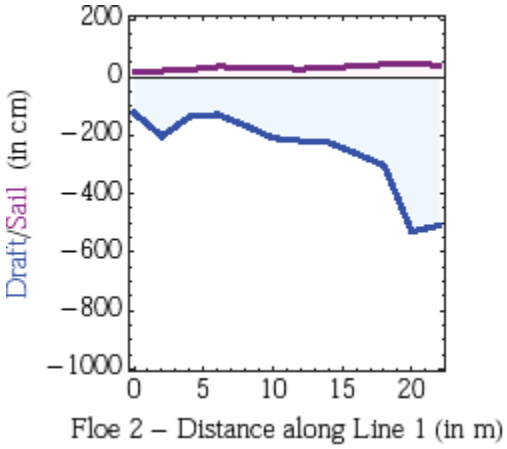

Floe 2 ALine

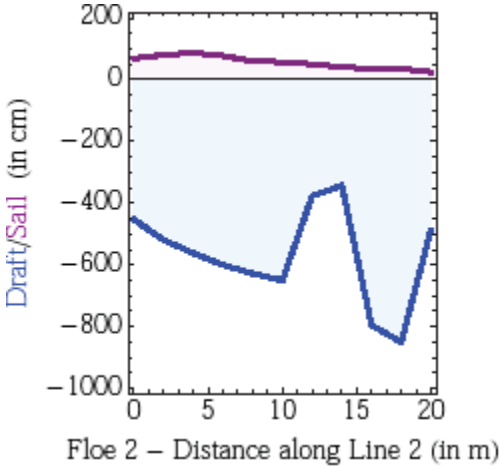

Floe 2 BLine

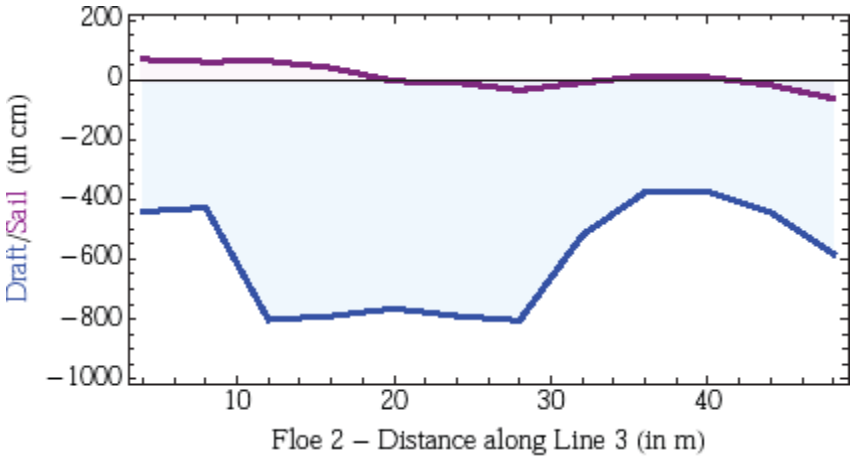

Floe 2 CLine

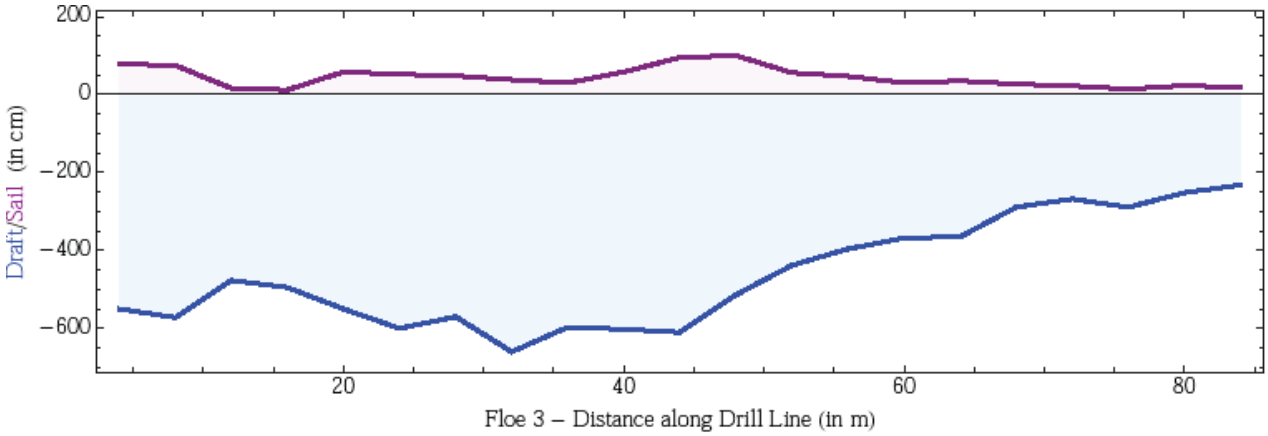

Floe 3 ALine

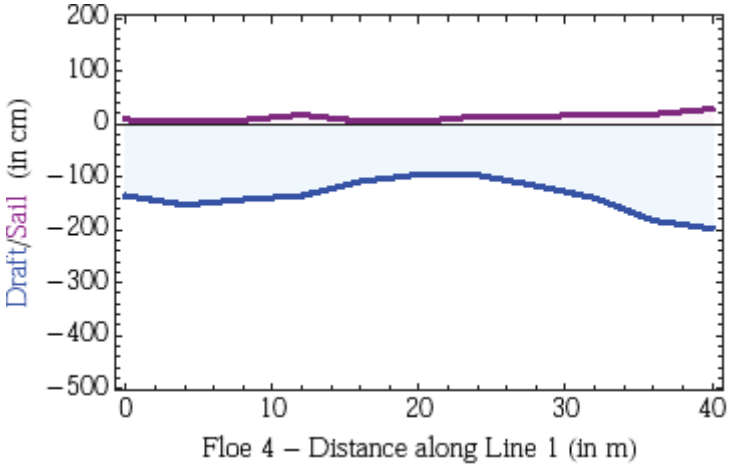

Floe 4 ALine

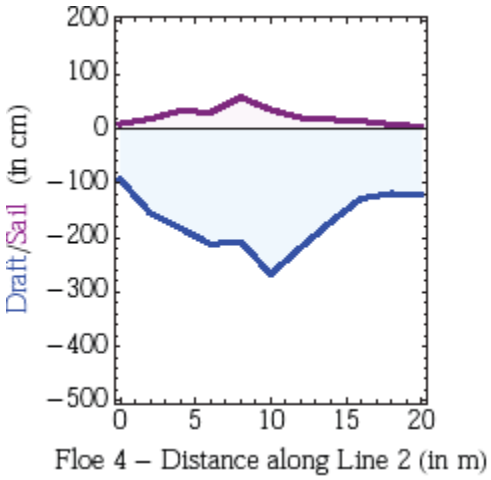

Floe 4 BLine

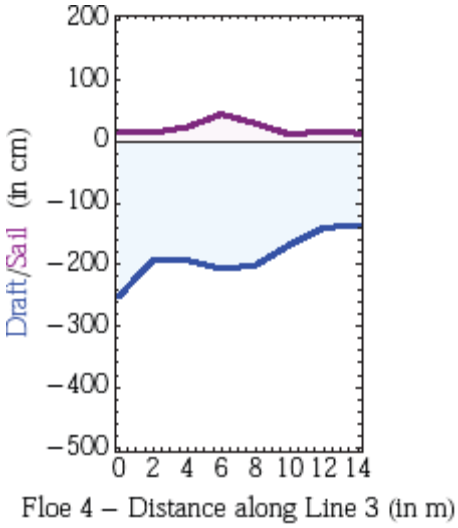

Floe 4 CLine

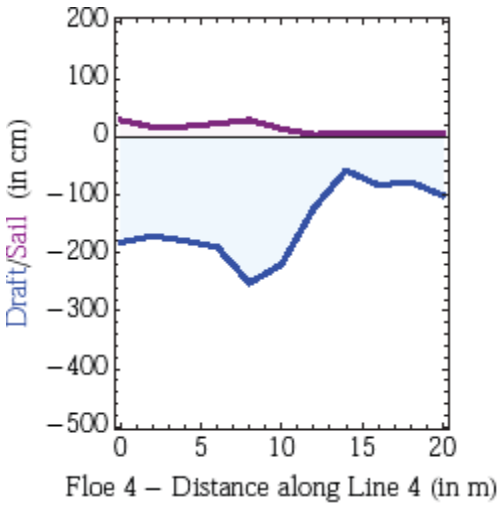

Floe 4 DLine

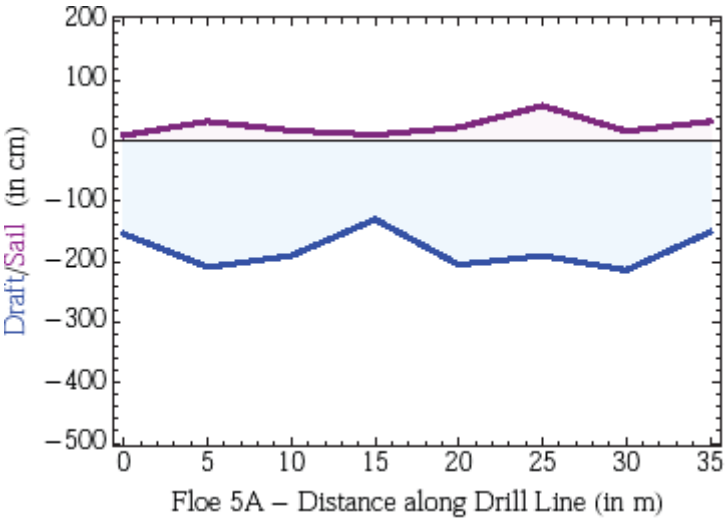

Floe 5A

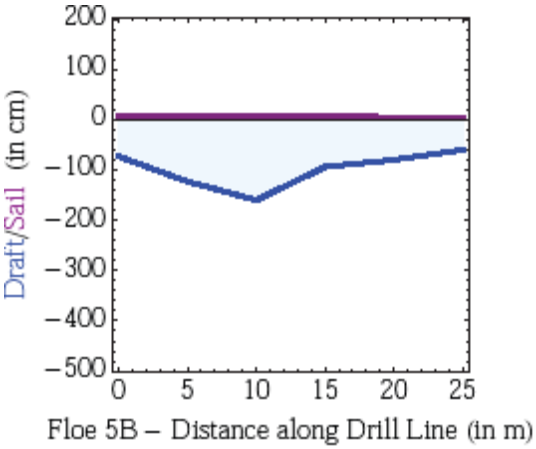

Floe 5B

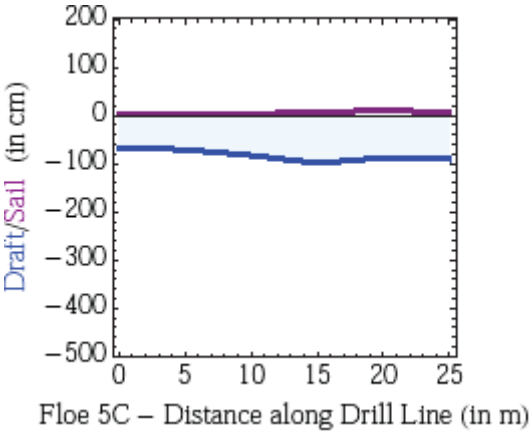

Floe 5C

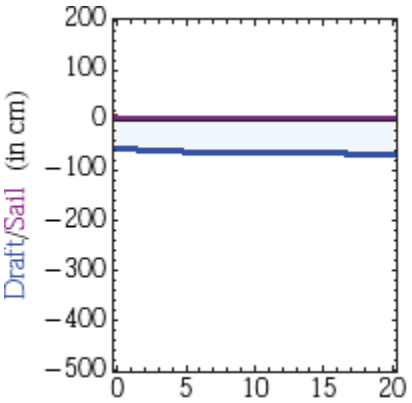

Floe 5D – Distance along Drill Line (in m)

Floe 5D

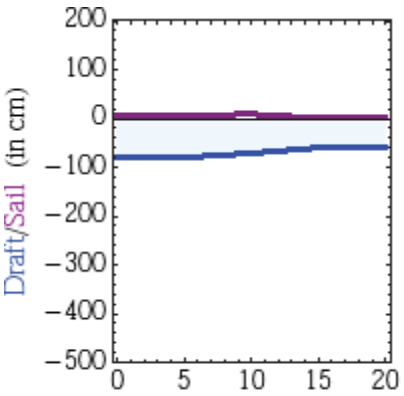

Floe 5E – Distance along Drill Line (in m)

Floe 5E

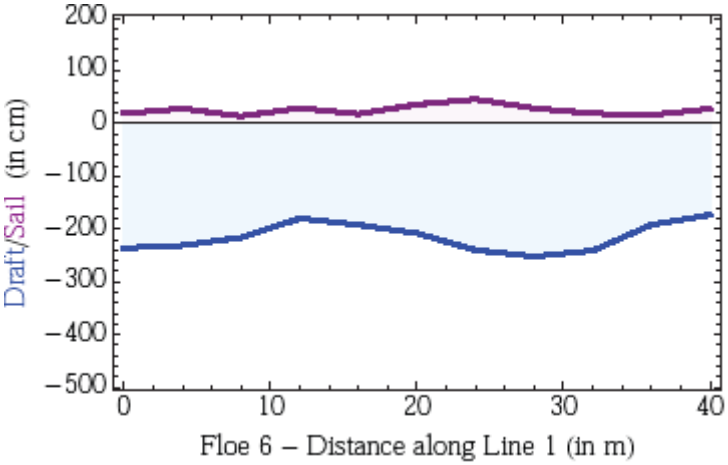

Floe 6 – Distance along Line 1 (in m)

Floe 6 ALine

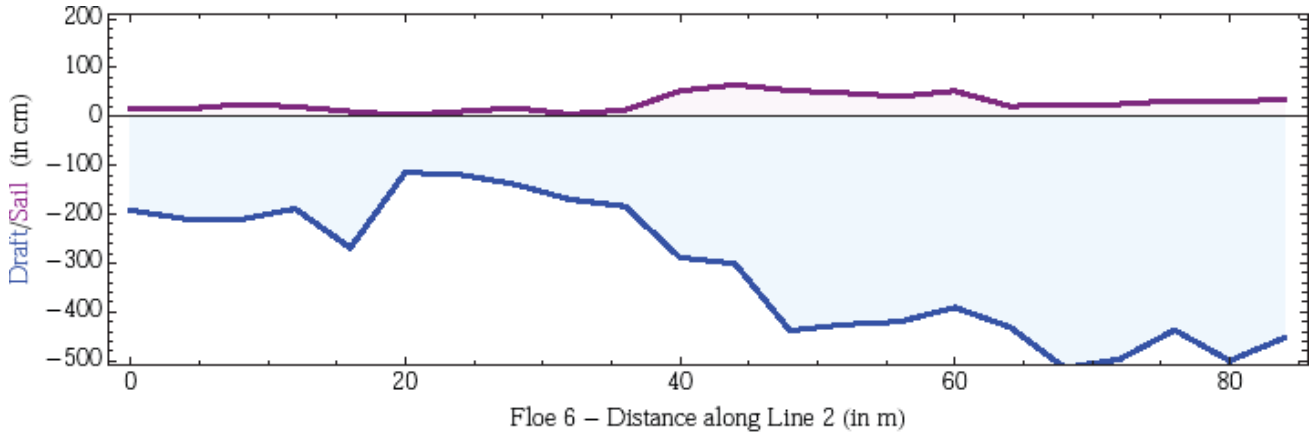

Floe 6 BLine

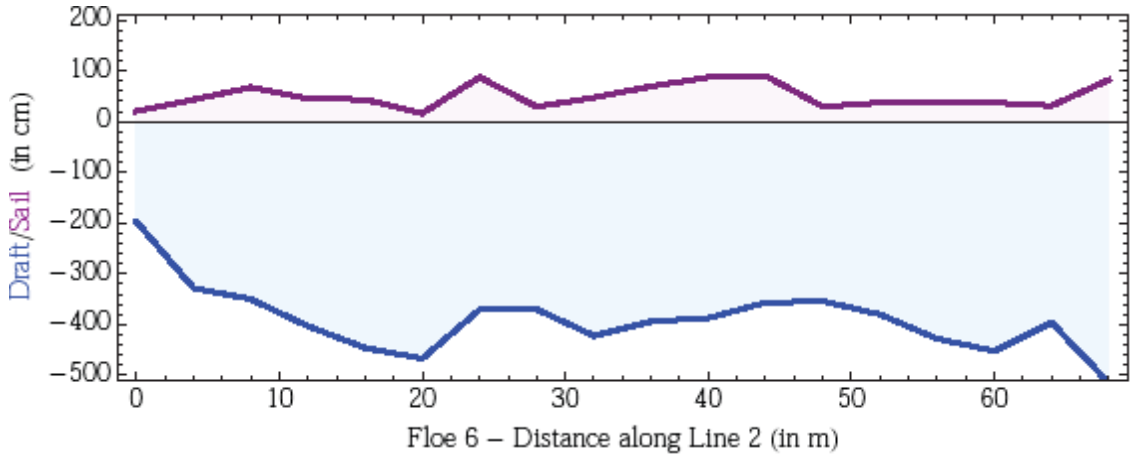

Floe 6 CLine

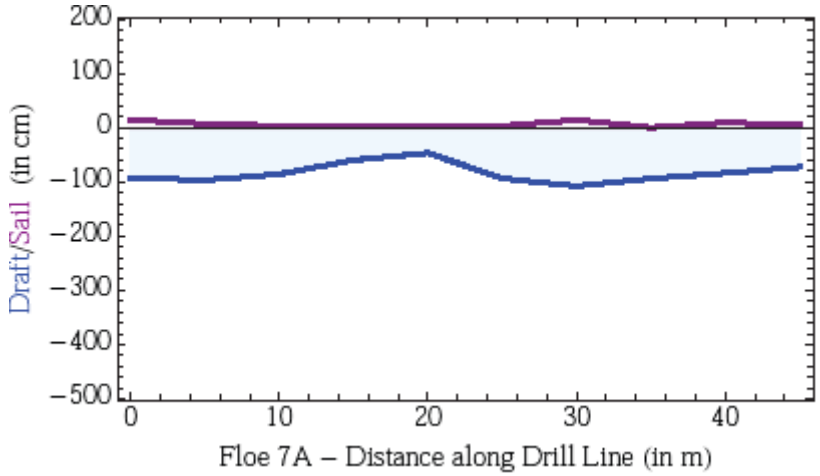

Floe 7A

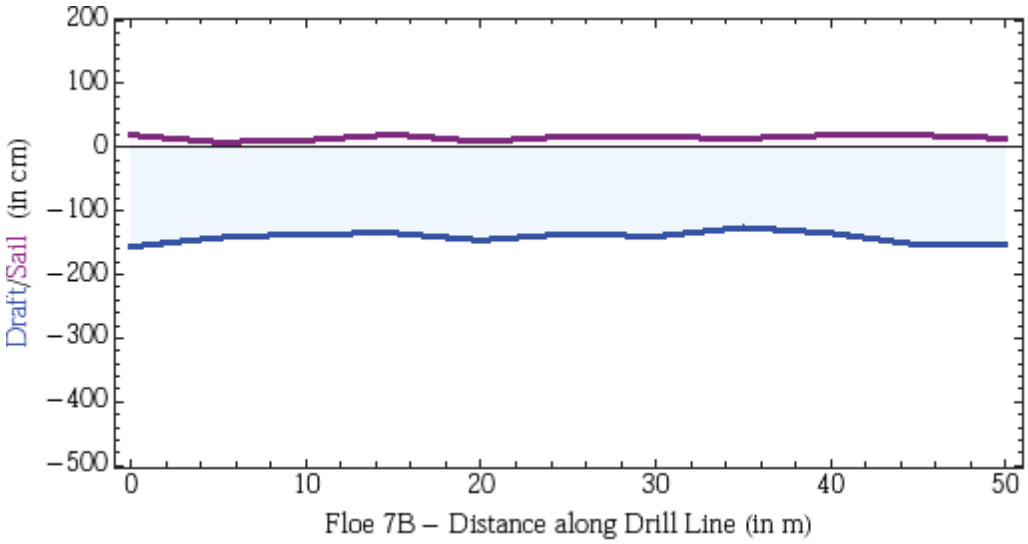

Floe 7B

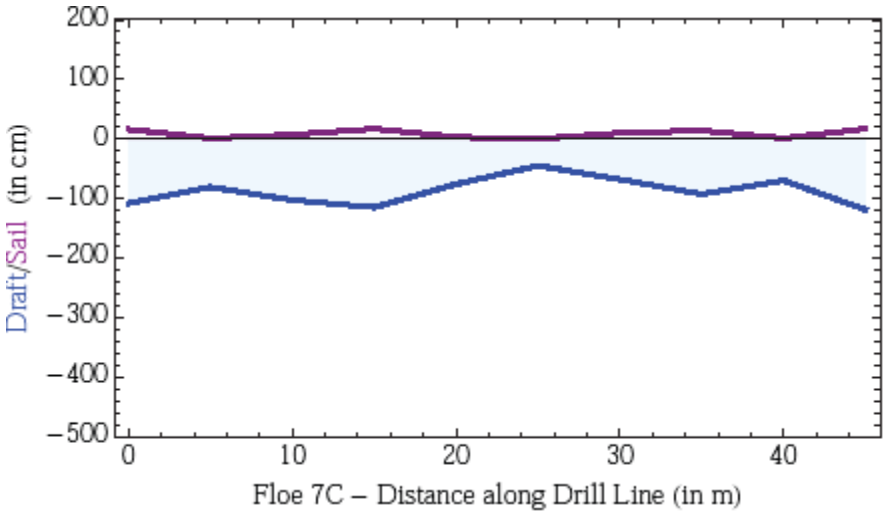

Floe 7C

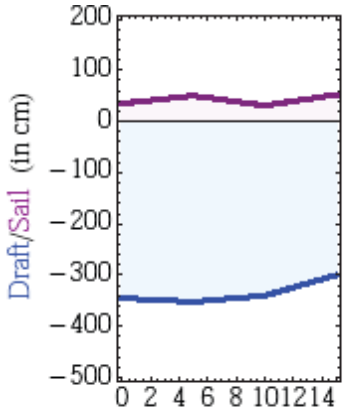

Floe 7D

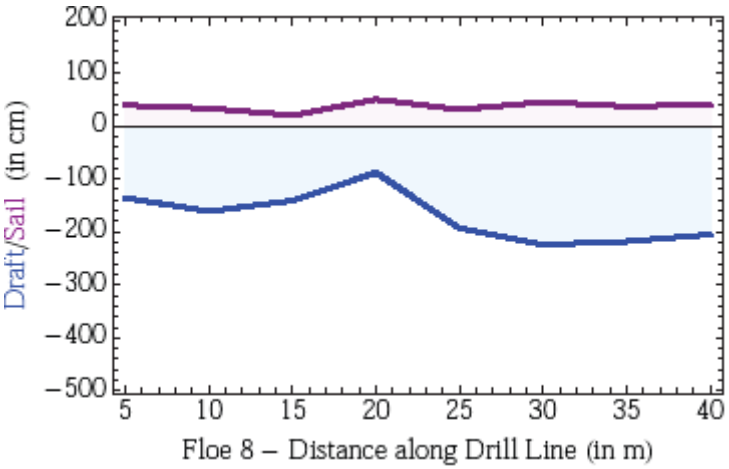

Floe 8

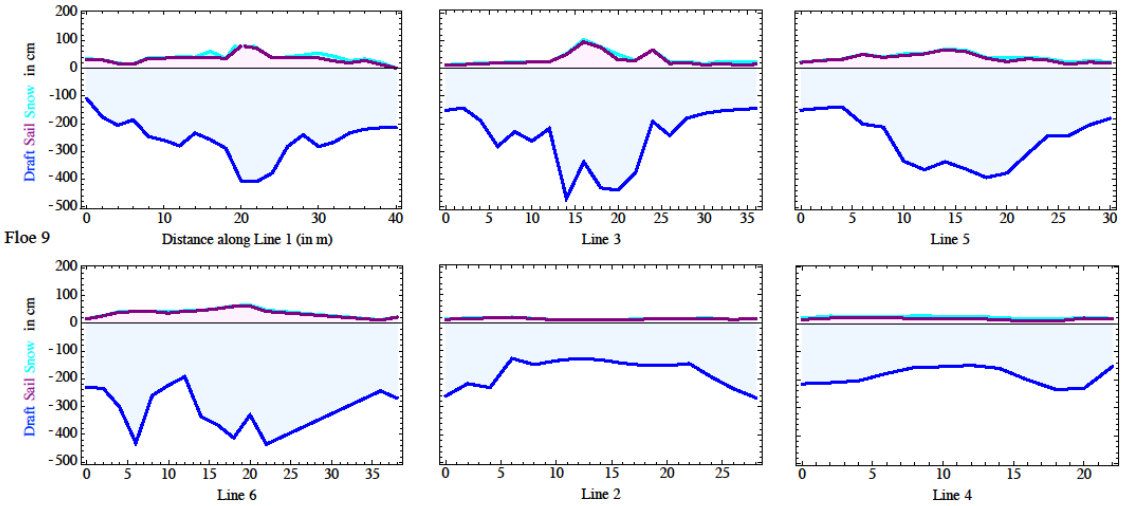

Floe 9 All Lines

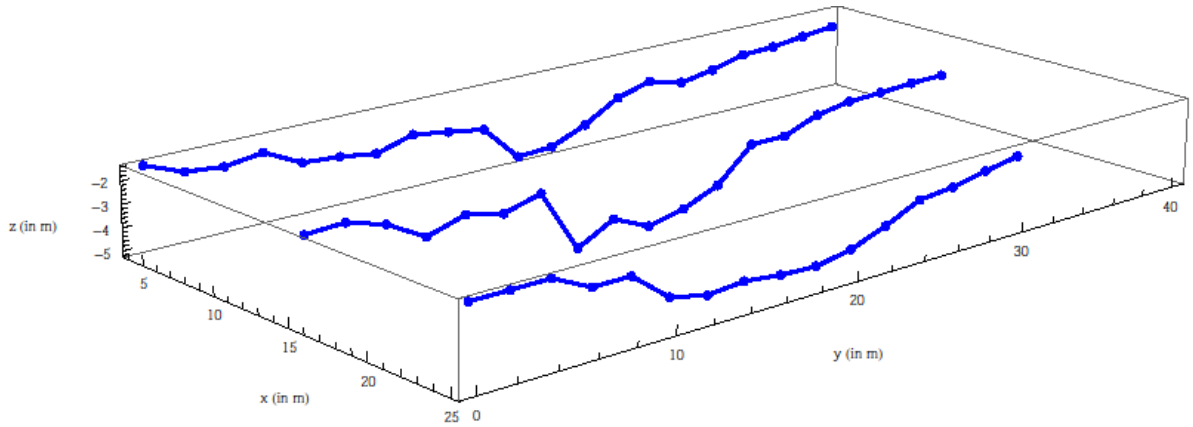

Floe 9 3D

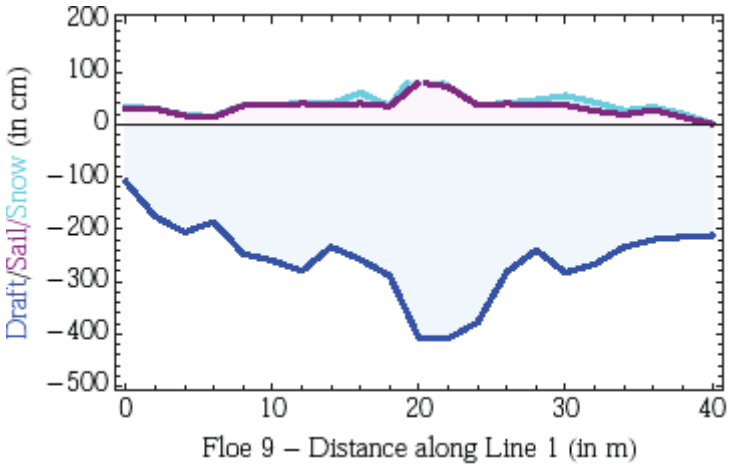

Floe 9 Line 1

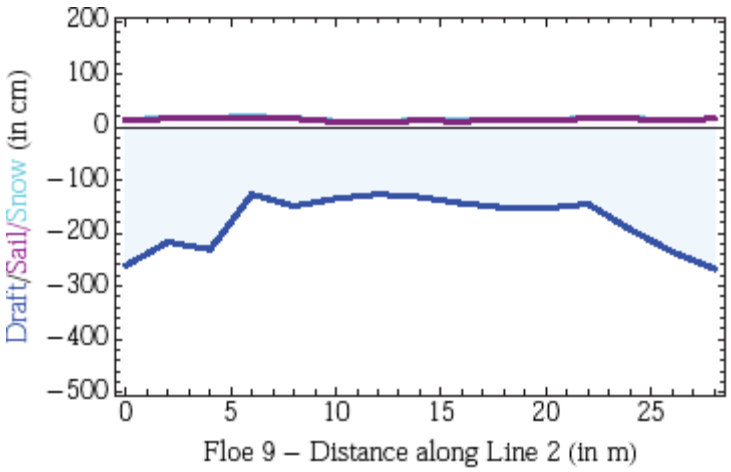

Floe 9 Line 2

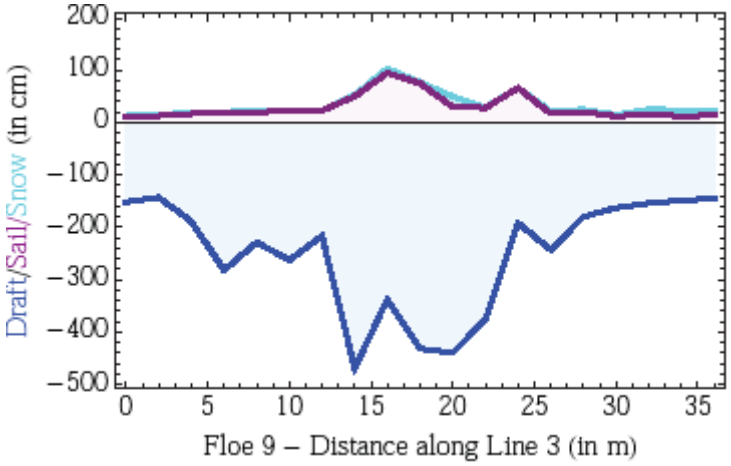

Floe 9 Line 3

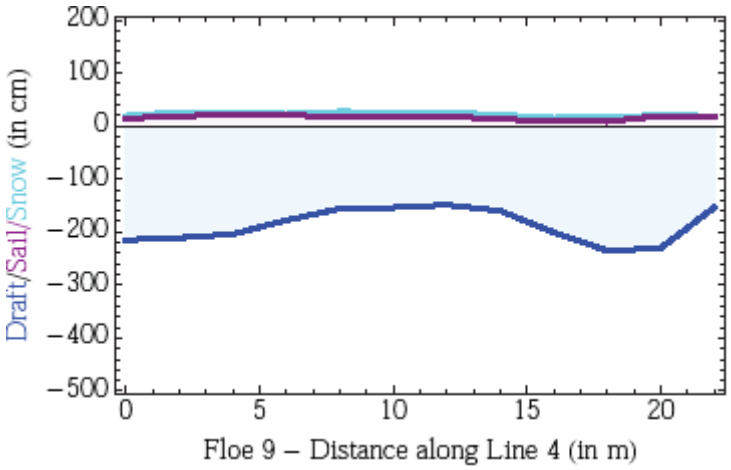

Floe 9 Line 4

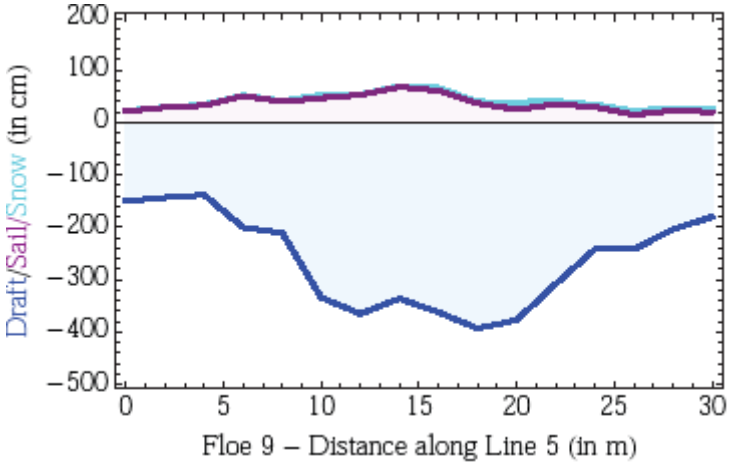

Floe 9 Line 5

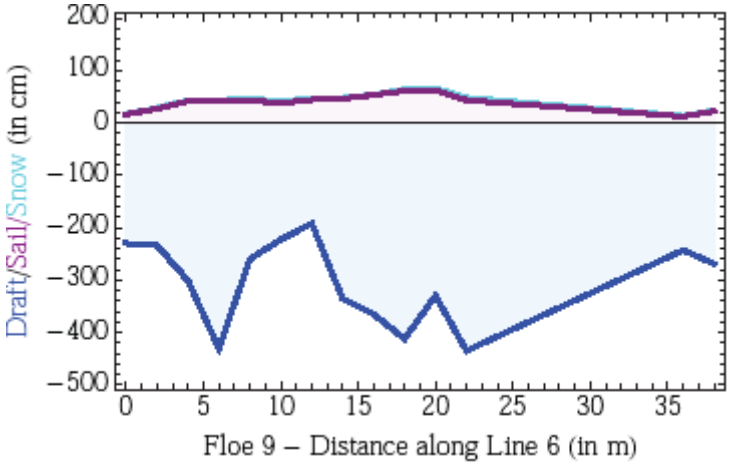

Floe 9 Line 6

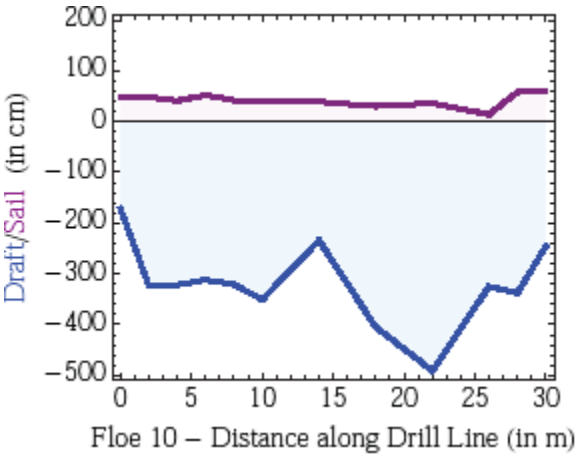

Floe 10 ALine

END OF DOCUMENT